Global and Planetary Change 246 (2025) 104732

Contents lists available at ScienceDirect

Global and Planetary Change

journal homepage: www.elsevier.com/locate/gloplacha

Size-fractionated C:N:P:Si stoichiometry of particulate matter in the subtropical Western North Pacific

Chaoyong Wang [a,b,1], Kan Zhang [a,b,1], Zhimian Cao [a,b,*], Kuanbo Zhou [a,b,*], Zhongwei Yuan [a,b], Junhui Chen [a,b], Yifan Ma [a,b], Bei Zhou [a,b], Xin Liu [a,c], Yihua Cai [a,b], Dalin Shi [a,b], Minhan Dai [a,b]

[a] State Key Laboratory of Marine Environmental Science, Xiamen University, Xiamen 361102, China
[b] College of Ocean and Earth Sciences, Xiamen University, Xiamen 361102, China
[c] College of the Environment and Ecology, Xiamen University, Xiamen 361102, China

ARTICLE INFO

Editor: Dr. Sun Jimin

Keywords:
C:N:P:Si stoichiometry
size-fractionated biogenic particles
phytoplankton community composition
subtropical western North Pacific

ABSTRACT

Particulate C:N:P:Si ratios and their variations in the upper ocean are crucial for understanding carbon export and its coupling with nutrient dynamics and phytoplankton community composition associated with nutrient limitation. Here, we present the first dataset of size-fractionated biogenic particle concentrations and their elemental ratios, including particulate organic carbon (POC), particulate nitrogen (PN), particulate phosphorus (PP), and biogenic silica (BSi), in the upper 500 m of the water column in the subtropical western North Pacific. The highest POC, PN, and PP concentrations consistently occurred in surface water and then decreased with increasing depth, whereas BSi concentration was frequently highest in the subsurface chlorophyll maximum layer at ~ 120 m. The small size fraction (SSF, 0.8 or 1–51 μm) dominated the total pool of POC, PN, and PP but contributed less to the total BSi pool than the large size fraction (LSF, >51 μm). This feature was accompanied by lower C:N, C:P, and N:P ratios and higher C:Si ratios in the SSF than in the LSF. In the euphotic zone, total particulate C:N, C:P, N:P, and C:Si ratios averaged 8 ± 1, 146 ± 30, 17 ± 3, and 120 ± 48 mol:mol respectively, and exceeded the canonical Redfield and Brzezinski ratio. The three former ratios aligned with cellular C:N:P ratios of *Prochlorococcus* and *Synechococcus*. Moreover, these ratios exhibited observable latitudinal gradients; they were generally higher in the gyre center than in its southern boundary occupied by the North Equatorial Current. Below the euphotic zone down to 500 m, there was a distinct increase in SSF molar C:N, C:P, and N:P ratios with depth, while total particulate molar C:Si ratios remained relatively constant. Combined with data collected in the subtropical eastern South Pacific and North Atlantic, our results demonstrate that the composition of the phytoplankton community primarily controls particulate molar C:N:P:Si stoichiometry in the euphotic zone of ocean gyres, in particular in the SSF, below which preferential remineralization of various bioelements plays an important role.

1. Introduction

Particles in seawater act as a vector for the transfer of atmospheric carbon dioxide (CO_2) and dissolved nitrogen (N), phosphorus (P), and silicon (Si) from the sunlit surface to the deep ocean via the biological pump, which plays an important role in the oceanic cycling of both carbon (C) and nutrients (Broecker and Peng, 1982; Subhas et al., 2023). The elemental stoichiometry of marine biogenic particles is considered to adopt an average value, known as the Redfield C:N:P ratios (106:16:1; Redfield, 1934) and Brzezinski C:Si ratio (106:15; Brzezinski, 1985), which forms a fundamental basis for understanding nutrient limitation patterns (Bonachela et al., 2013; Alexander et al., 2015), coupling of nutrient and C cycles (DeVries and Deutsch, 2014), and the dynamics of C export from the euphotic zone under climate change (Matsumoto et al., 2020a; Matsumoto and Tanioka, 2020).

An increasing number of studies have so far revealed both spatial and temporal variations in particulate C:N:P ratios (Sterner et al., 2008; Martiny et al., 2013a; Martiny et al., 2013b; Quay, 2021) and particulate

* Corresponding authors at: State Key Laboratory of Marine Environmental Science, Xiamen University, Xiamen 361102, China.
E-mail addresses: zmcao@xmu.edu.cn (Z. Cao), kbzhou@xmu.edu.cn (K. Zhou).
[1] C. Wang and K. Zhang contributed equally to this work.

https://doi.org/10.1016/j.gloplacha.2025.104732
Received 23 February 2024; Received in revised form 19 December 2024; Accepted 27 January 2025
Available online 28 January 2025

C:Si ratio (Ragueneau et al., 2006) in the upper ocean. Field observations demonstrated that particulate C:N, C:P, and N:P and particulate C:Si ratios generally exceed the Redfield and Brzezinski ratio, respectively, in the subtropical ocean, whereas at high-latitude and in equatorial upwelling regions they typically display lower values (Arrigo et al., 2002; Martiny et al., 2013a). Inverse ocean biogeochemistry models have inferred a similar spatial pattern of global particulate C:P and N:P ratios (Teng et al., 2014; Wang et al., 2019).

Overall, variations in particulate C:N:P ratios are considered to be associated with changes in the composition of the phytoplankton community and in environmental conditions (Martiny et al., 2013b; Baer et al., 2017; Matsumoto et al., 2020b; Tanioka and Matsumoto, 2020). Oligotrophic ocean gyres, dominated by picocyanobacteria, generally have elevated particulate C:P and N:P ratios compared to eutrophic environments where larger eukaryotes, such as diatoms, typically thrive (Geider and Roche, 2002; Martiny et al., 2013a; Lomas et al., 2021). Laboratory culture experiments showed that dinitrogen (N_2) fixation by diazotrophs leads to increased particulate C:P and N:P ratios (Follett et al., 2018), while field observations at station ALOHA (A Long-Term Oligotrophic Habitat Assessment; 22.75°N, 158.00°W) demonstrated that diatom-diazotroph associations decrease particulate C:Si ratios (Brzezinski et al., 2011). Moreover, N limitation in the North Pacific can lead to high particulate C:N and C:P ratios and low N:P ratios relative to other ocean gyres (Van Mooy and Devol, 2008; Mouginot et al., 2015; Garcia et al., 2018). Increases in light intensity and temperature also potentially elevate particulate C:N and C:P ratios (Tanioka and Matsumoto, 2020).

The subtropical western North Pacific (wNP) is characterized by year-round near-surface stratification, depleted surface nutrients, and extremely low biological productivity mainly limited by N (Van Mooy and Devol, 2008; Wen et al., 2022; Dai et al., 2023). Picophytoplankters including *Prochlorococcus* and *Synechococcus* are dominant contributors to biomass and primary productivity in the euphotic zone (Browning et al., 2022; Zhang et al., 2024b). The subtropical wNP is overall an important sink of atmospheric CO_2 (Takahashi et al., 2009; Iida et al., 2021). However, our current understanding of particulate C:N:P:Si ratios and of their vertical variations in this region is relatively limited (Hebel and Karl, 2001; Lam et al., 2018), hampering the precise evaluation of biological pump efficiency. In addition, strong N_2 fixation has been observed in the center of the wNP subtropical gyre (Shiozaki et al., 2010; Tang et al., 2019; Gradoville et al., 2020; Wen et al., 2022; Shao et al., 2023), whereas its influence on particulate C:N:P:Si stoichiometry remains unknown.

In this study, size-fractionated biogenic particle samples, including particulate organic carbon (POC), particulate nitrogen (PN), particulate phosphorus (PP), and biogenic silica (BSi), were collected in three zones (the Kuroshio Current (KC), North Pacific Subtropical Gyre (NPSG), and North Equatorial Current (NEC)) of the subtropical wNP (Fig. 1). Based on this field sampling, we systematically examine the lateral and vertical distributions of biogenic particle concentrations and C:N:P:Si ratios in the upper 500 m of the water column. These results are further integrated with previous findings from both culture experiments of phytoplankton species and from field observations in the subtropical eastern South Pacific (eSP) and North Atlantic (NA), in order to explore the factors controlling particle composition in oligotrophic ocean gyres.

2. Methods

2.1. Study area

The subtropical wNP borders the eastern portion of the Asian continent and belongs to the largest gyre in the world's ocean, the NPSG. Major surface currents in the subtropical wNP include a coherent westward-flowing current, the NEC driven by the trade winds near 10°N, along with its bifurcations, the northward-flowing KC and the southward-flowing Mindanao Current, along the eastern Philippine coast (Fig. 1). The subtropical wNP is highly oligotrophic, with the lowest surface chlorophyll-*a* (Chl- *a*) and nutrient concentrations in the global ocean, and is often regarded as an "ocean desert" (Chow et al., 2019; Matsumoto et al., 2021). Bulk phytoplankton growth in this region is primarily limited by N, secondarily by P or iron (Fe), depending on their rates of supply to the euphotic zone (Li et al., 2015; Browning et al., 2022; Yuan et al., 2023). Moreover, the north-south gradient of these rates results in pronounced latitudinal variability in N_2 fixation rates (Hashihama et al., 2009; Kitajima et al., 2009; Wen et al., 2022). Despite low primary productivity, the extensive area of the subtropical wNP makes it an important zone for the export of biogenic particles to the deep ocean (Winn et al., 1994; Liu et al., 2020).

2.2. Cruise and sampling

Sampling was conducted at 13 stations during the GEOTRACE-GP09 cruise, onboard the R/V *Tan Kah Kee*, from April 25 to June 13, 2019 in the subtropical wNP (Browning et al., 2022; Wen et al., 2022; Zhang

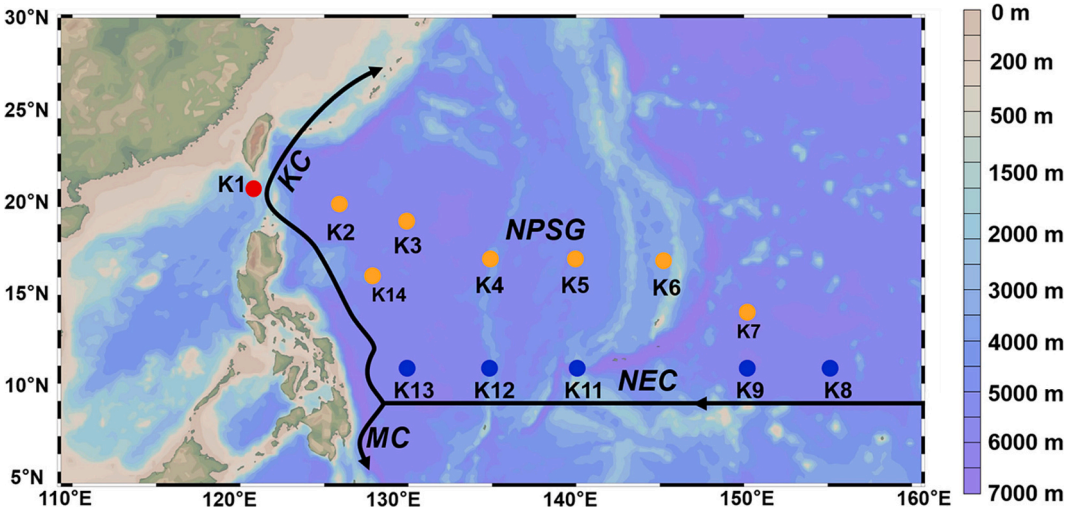

Fig. 1. Map of the western North Pacific (wNP) showing sampling stations where in-situ pumps were deployed during the 2019 GEOTRACES-GP09 cruise. The North Pacific Subtropical Gyre (NPSG) zone includes stations K2 to K7 and K14 (yellow circles), the North Equatorial Current (NEC) zone includes stations K8 to K13 (blue circles), and station K1 (red circle) is influenced by the Kuroshio Current (KC). Major surface currents, including the NEC, KC, and Mindanao Current (MC), are also schematically depicted. (For interpretation of the references to colour in this figure legend, the reader is referred to the web version of this article.)

et al., 2024b). Station K1 in the Luzon Strait was situated along the KC pathway. The NPSG zone included stations K2 to K7 and K14, and the NEC zone included stations K8 to K13 (Fig. 1).

During the cruise, size-fractionated particulate samples were collected from the upper 500 m of the water column using modified large-volume, dual-flow McLane Research in-situ pumps (WTS-LV) at each sampling station. A 51 μm Sefar polyester mesh prefilter was used, followed by 1 μm Whatman QMA quartz fiber filters and 0.8 μm Pall Supor800 polyethersulfone (PES) filters, respectively, on two filter holders (A side for QMA filters and B side for PES filters). Six to eight pumps per cast operated for 3 to 5 h and ~ 1000 L of seawater were filtered by each pump, with ~ 400 and ~ 600 L through the A and B side, respectively. Particles larger than 51 μm were categorized as the large size fraction (LSF), while those ranging from 0.8 or 1 to 51 μm were defined as the small size fraction (SSF). SSF POC and PN samples (POC_{SSF} and PN_{SSF}, respectively) were taken from the QMA filter on the A side, while SSF PP and BSi samples (PP_{SSF} and BSi_{SSF}, respectively) were taken from the PES filter on the B side. Except for LSF PP samples (PP_{LSF}) obtained from the mesh prefilter on the B side, LSF POC, PN, and BSi samples (POC_{LSF}, PN_{LSF}, and BSi_{LSF}) were obtained from the mesh prefilter on the A side. Total particle concentration is the sum of the two size fractions, e.g., $POC_{Total} = POC_{SSF} + POC_{LSF}$.

2.3. Analysis of biogenic particles

2.3.1. Particulate organic carbon and nitrogen

Samples for POC and PN determination were oven-dried at 50 °C for 24 h and soaked in a 1 mol L^{-1} HCl solution for ca. 5 min to remove carbonate. Subsequently, they were dried again at 50 °C overnight and pelletized in tin discs. POC and PN concentrations, as well as the PN stable N isotopic composition ($\delta^{15}N_{PN}$), were measured using an elemental analyzer-isotope ratio mass spectrometer (vario PYRO cube + Isoprime 100). In each batch run, measurements of international (USGS 40, L-glutamic acid with $\delta^{15}N$ of −4.5 ± 0.1 ‰) and working (acetanilide with $\delta^{15}N$ of −1.5 ± 0.2 ‰, Merck) standards were inserted into every five to six samples.

For POC and PN concentration measurements, the detection limit was defined as 3 times the standard deviation (SD) of QMA filter blanks, which were pretreated and analyzed the same way as particle samples (Lam et al., 2018). All POC and PN contents in the digestion solution of SSF and LSF were above corresponding detection limits of 40 and 4.6 μg, respectively. Note that due to minor fractions of particulate inorganic N in open ocean waters (Feng et al., 2018), PN represents the dominant organic component as suggested by Pujo-Pay et al. (2011), Piper et al. (2016), and Lam et al. (2018). The precision for both POC and PN concentrations was <10 % (Zhou et al., 2013), and for $\delta^{15}N_{PN}$ it was <0.2 ‰ (Yang et al., 2017).

2.3.2. Particulate phosphorus

Samples for PP determination, as well as dipped blanks that are polyester mesh prefilter + PES filter placed in a perforated acid-cleaned plastic container attached to the in-situ pump frame, were dried at room temperature and subsequently digested using a HNO_3-HF reflux method (Ohnemus et al., 2014; Lee et al., 2018), followed by analyzing on a Thermo Scientific Element XR HR-ICP-MS system. The detection limit of the measurement was 3 times the SD of dipped blanks, which were 39.2 and 71.9 nmol, respectively, for SSF and LSF. Note that most PP_{LSF} contents in the digestion solution of samples between 200 and 500 m were below the detection limit, and thus the derived in-situ concentration data were considered unreliable and excluded. Similar to the usage of term PN, PP represents the dominant organic component as suggested by Pujo-Pay et al. (2011), Piper et al. (2016), and Lam et al. (2018). Long-term measurements of PP in the certified reference material BCR-414 (a plankton powder; 14,027 ± 727 μg g^{-1}, $n = 20$) yielded a precision of 5 % as the relative SD. Details about the analysis procedure were described by Zhang et al. (2024b), in which PP concentration data have been presented.

2.3.3. Biogenic silica

Samples for BSi determination were dried at 50 °C for 24 h and leached using 4 mL of 0.2 M NaOH at 100 °C for 40 min according to the one-step wet-alkaline digestion method (Lam et al., 2018). Concentrations of Si in the digestion solution were determined by spectrophotometric detection of the blue silico-molybdate complex using a Technicon AA3 Auto-Analyzer (Bran + Luebbe GmbH). Measurements of dipped blanks for both SSF and LSF BSi indicated near-zero Si content in the digestion solution. Extremely low aluminum concentrations ruled out any important contributions from lithogenic silica. Repeated measurements of selected filter samples yielded an uncertainty for the entire procedure of <10 % (Cao et al., 2020).

3. Results

3.1. Vertical distribution of biogenic particle concentrations above 500 m

3.1.1. Particulate organic carbon and nitrogen

High POC_{SSF} (1–51 μm) concentrations were consistently observed in the euphotic zone (spanning from the surface to a depth corresponding to 1 % photosynthetically active radiation at each sampling station), with an average value (± 1SD) of 0.93 ± 0.16 μmol L^{-1} (Figs. 2a and S1a, Table S1). Below the euphotic zone, POC_{SSF} concentrations declined rapidly and were almost uniformly distributed between 200 and 500 m, averaging 0.20 ± 0.04 μmol L^{-1}. In contrast, POC_{LSF} (>51 μm) ranged from 0.01 to 0.48 μmol L^{-1} in surface water (Figs. 2b and S1e). The average POC_{LSF} concentration in the euphotic zone (0.11 ± 0.09 μmol L^{-1}) was nearly one order of magnitude lower than that of POC_{SSF}. Below the euphotic zone, POC_{LSF} concentrations also declined with increasing depth and remained relatively uniform between 200 and 500 m (on average 0.03 ± 0.01 μmol L^{-1}). Due to the predominant contribution of POC_{SSF} to POC_{Total} (>1 μm), the latter's concentration distribution was very consistent with that of the former (Fig. 2a and c).

Vertical distributions of PN exhibited similar patterns to those of POC. The average concentration of PN_{SSF} and PN_{LSF} was 111.4 ± 18.7 nmol L^{-1} and 11.2 ± 9.9 nmol L^{-1}, respectively, in the euphotic zone, below which both concentrations decreased with increasing depth down to 500 m (Figs. 2d and e and S1b and f, Table S1). Because PN_{SSF} contributed to most of the PN_{Total}, the latter's distribution pattern aligned with that of the former.

3.1.2. Particulate phosphorus

Concentrations of PP_{SSF} (0.8–51 μm) were relatively high in the euphotic zone, with an average value (± 1SD) of 6.6 ± 1.3 nmol L^{-1}. Subsequently, PP_{SSF} rapidly decreased to a constant level, averaging 2.3 ± 1.9 nmol L^{-1} below the euphotic zone (Figs. 3a and S1c, Table S1). PP_{LSF} (>51 μm) concentrations in the euphotic zone, with an average value of 0.4 ± 0.3 nmol L^{-1}, were on average 16.5 (~ 6.6/0.4) times lower than those of PP_{SSF}. Between 200 and 500 m, most PP_{LSF} contents in digestion solutions were below the detection limit suggesting near-zero in-situ concentrations (Figs. 3b and S1g). PP_{Total} (>0.8 μm) concentrations were only calculated in the euphotic zone with an average value of 7.1 ± 1.3 nmol L^{-1} (Fig. 3c).

3.1.3. Biogenic silica

The vertical distribution of BSi concentrations contrasted notably with those of POC, PN, and PP. At individual stations, the highest BSi concentration was not always confined to surface water but could extend down to 200 m (Figs. 3d and e and S1d and h, Table S1). Specifically, BSi_{SSF} (0.8–51 μm) was primarily concentrated between 100 and 200 m at stations K8 to K13 in the NEC zone (Fig. 3d). Overall, vertical distributions of BSi_{LSF} (>51 μm) followed those of BSi_{SSF}, whereas the former showed a slightly higher average value than the latter above 500

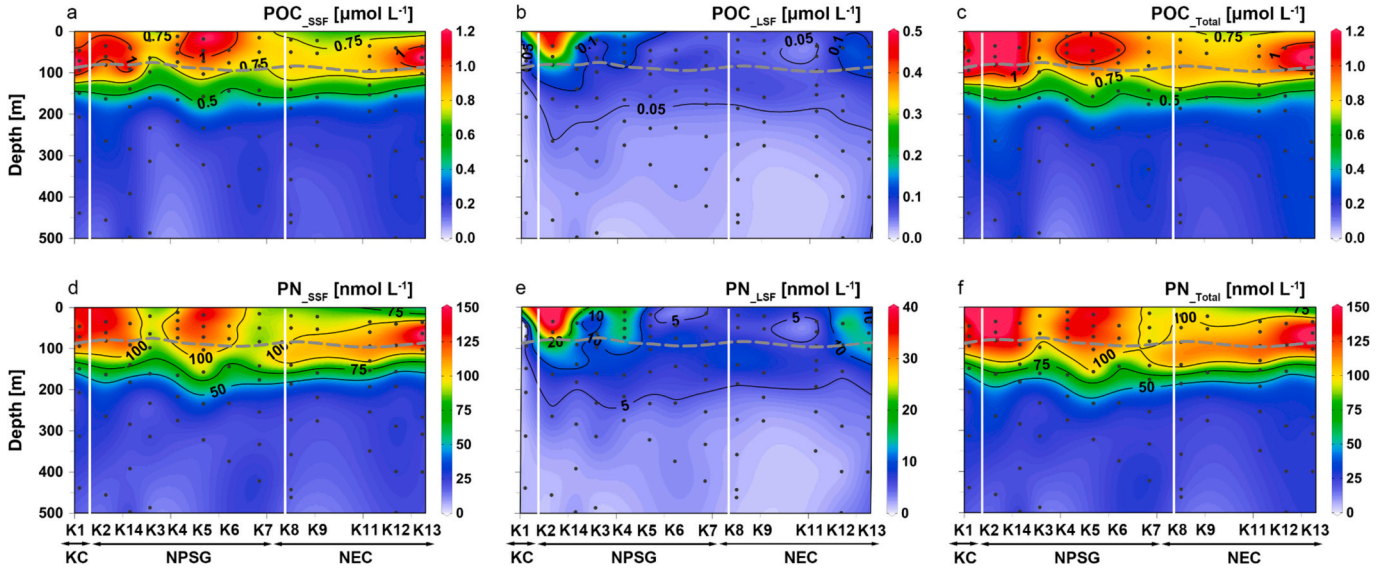

Fig. 2. Distribution of (a-c) particulate organic carbon, POC and (d-f) particulate nitrogen, PN concentrations in the upper 500 m of the water column. Left: small size fraction (SSF, 1–51 μm); middle: large size fraction (LSF, >51 μm); right: total particulates (Total, >1 μm). White lines in each plot separate the Kuroshio Current (KC), North Pacific Subtropical Gyre (NPSG), and North Equatorial Current (NEC) zone, and the gray dashed line indicates the bottom of the euphotic zone.

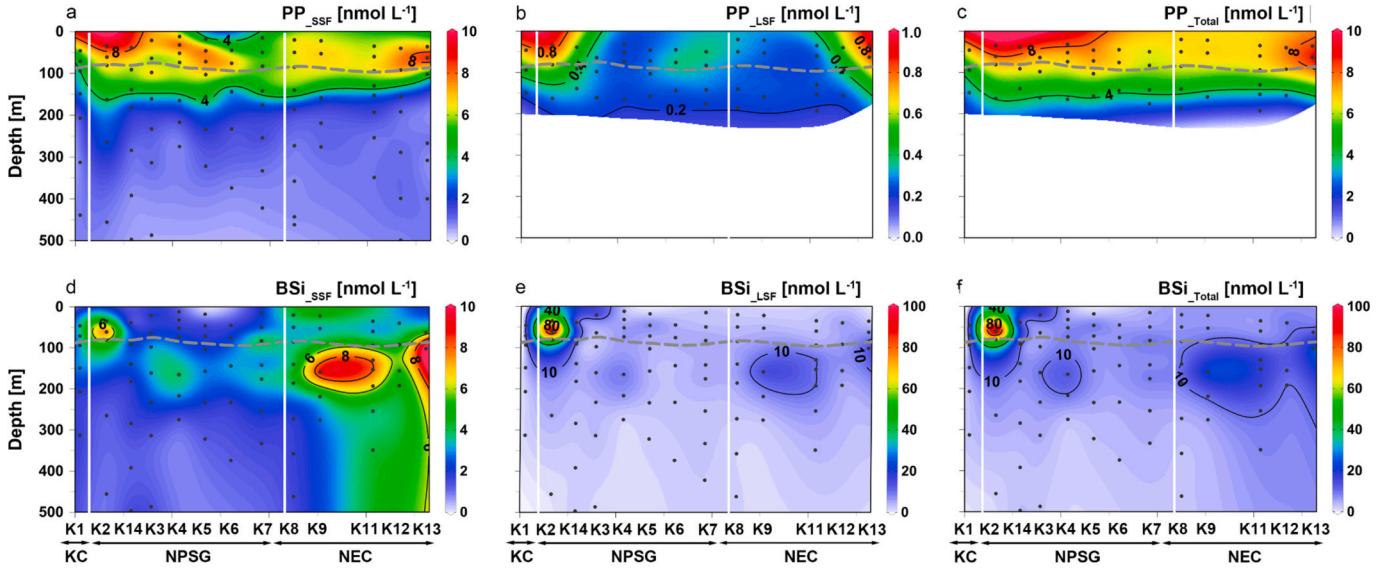

Fig. 3. Distribution of (a-c) particulate phosphorus, PP and (d-f) biogenic silica, BSi concentrations in the upper 500 m of the water column. Left: small size fraction (SSF, 0.8–51 μm); middle: large size fraction (LSF, >51 μm); right: total particulates (Total, >0.8 μm). Note that the majority of LSF PP measurements between 200 and 500 m were below the detection limit. White and gray lines in each panel are depicted in the caption of Fig. 2.

m (7.6 ± 14.7 vs. 3.2 ± 2.2 nmol L^{-1}). It is noteworthy that an extremely high BSi_{LSF} concentration of 114.5 nmol L^{-1} was observed at around 60 m at station K2 (Fig. 3e). This value mainly induced larger 1SD of 14.7 than the corresponding average of 7.6, indicating pronounced spatial variability of BSi_{LSF} among sampling stations. In contrast to the size-fractionated composition of POC, PN, and PP, BSi_{LSF} represents a more important contribution than BSi_{SSF} to BSi_{Total}. Therefore, the distribution pattern of BSi_{Total} (>0.8 μm) largely followed that of BSi_{LSF} (Fig. 3f).

3.2. Vertical distribution of particulate molar C:N:P:Si ratios above 500 m

3.2.1. Particulate molar C:N ratios

$C:N_{SSF}$ ratios varied from 7 to 9 mol:mol, attaining a median of ~ 8 mol:mol in the euphotic zone (Fig. 4a, Table S2). $C:N_{LSF}$ ratios were generally <10 mol:mol in the euphotic zone, and then increased rapidly with depth down to 500 m, with an average value (± 1SD) of 11 ± 2 mol:mol excluding data collected at stations K4 to K6. At these three stations, $C:N_{LSF}$ ratios were uniformly low throughout the entire depth profile (Fig. 4b). The distribution pattern of $C:N_{Total}$ ratios again reflected those of $C:N_{SSF}$ ratios above 500 m, with an average value of 8 ± 1 mol:mol, which was somewhat higher than the Redfield ratio of 6.6 mol:mol (Redfield, 1934) (Fig. 4c).

3.2.2. Particulate molar C:P ratios

$C:P_{SSF}$ ratios were on average lower in the euphotic zone (140 ± 33 mol:mol) than in waters below (189 ± 61 mol:mol), excluding values for station K5, where the former average $C:P_{SSF}$ was within errors consistent with or slightly higher than the Redfield ratio of 106 mol:mol

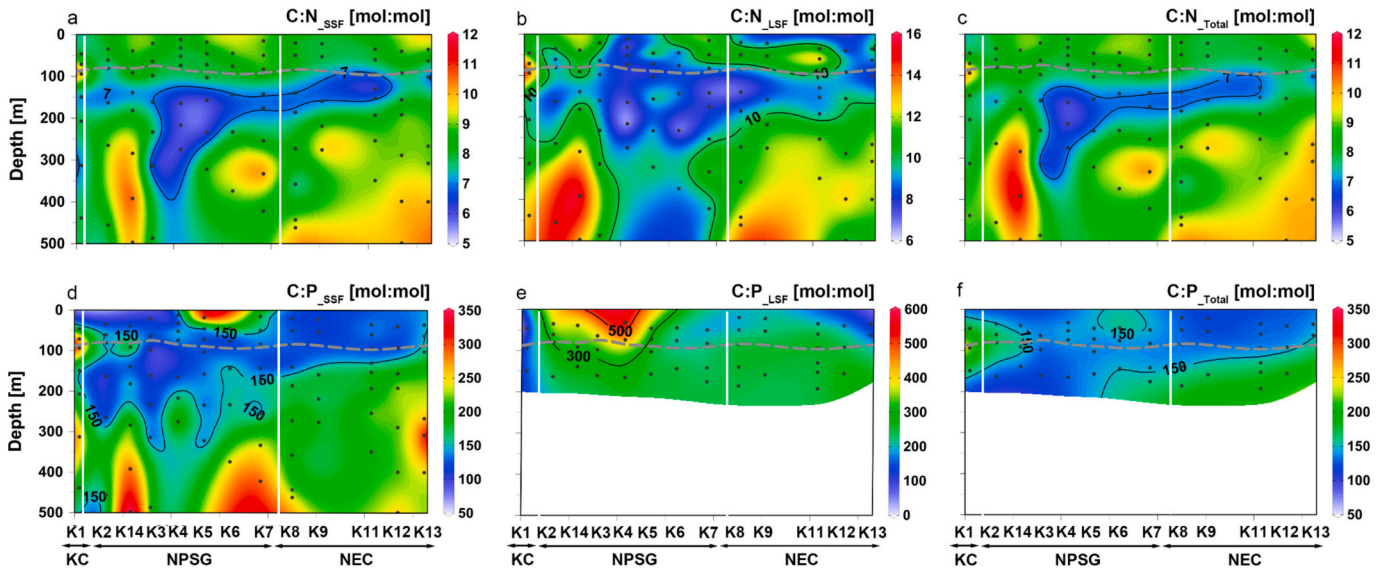

Fig. 4. Distribution of particulate ratios (a-c) C:N and (d-f) C:P in the upper 500 m of the water column. Left: small size fraction (SSF, 0.8 or 1–51 μm); middle: large size fraction (LSF, >51 μm); right: total particulates (Total, >0.8 or 1 μm). Since particulate P concentrations in the LSF were mostly below the detection limit between 200 and 500 m, $C:P_{LSF}$ and $C:P_{Total}$ ratios in these waters were not calculated. White and gray lines in each panel are depicted in the caption of Fig. 2.

(Redfield, 1934). Surface water at station K5 reached a relatively high $C:P_{SSF}$ ratio of 325 mol:mol. The 150 mol:mol contour, generally located between 200 and 300 m, was relatively deeper at stations K2 to K5, while it gradually became shallower from stations K7 to K13 (Fig. 4d, Table S2). The vertical distribution of $C:P_{LSF}$ ratios followed to some extent that of the $C:P_{SSF}$ ratio, but showed a much higher average value of 283 ± 149 mol:mol in the euphotic zone, notably surpassing the Redfield ratio (Fig. 4e). $C:P_{Total}$ ratios were only calculated in the euphotic zone with an average value of 146 ± 30 mol:mol, while their distribution patterns were nearly the same as those of $C:P_{SSF}$ ratios (Fig. 4d and f).

3.2.3. Particulate molar N:P ratios

The vertical distribution of $N:P_{SSF}$ ratios generally showed a similar pattern to that of the $C:P_{SSF}$ ratios. The average $N:P_{SSF}$ ratio was higher below the euphotic zone (23 ± 6 mol:mol) than in waters above (17 ± 3 mol:mol), excluding a peak value of 36 mol:mol at 18 m of station K5 (Fig. 5a, Table S2). The average $N:P_{LSF}$ ratio in the euphotic zone was 31 ± 21 mol:mol and exceeded the Redfield ratio of 16 mol:mol (Redfield, 1934), while high ratio values were mainly observed in the NPSG zone (Fig. 5b). $N:P_{Total}$ ratios above 200 m overall exhibited a vertical gradient, with larger values at greater depths (Fig. 5i), similar to that of the $N:P_{SSF}$ ratios. In the euphotic zone, $N:P_{Total}$ ratios ranged from 14 to 28 mol:mol, yielding an average value of 17 ± 3 mol:mol (Fig. 5c, Table S2), consistent with or slightly higher than the Redfield ratio. It is noteworthy that particulate molar C:N, C:P, and N:P ratios consistently pointed to the dominant contribution of small size-fractionated particles to the total organic "soft tissue" pool.

3.2.4. Particulate molar C:Si ratios

Ratios of $C:Si_{SSF}$ exhibited notably higher values in the euphotic zone, averaging 344 ± 153 mol:mol (Fig. 5d, Table S2). Below the

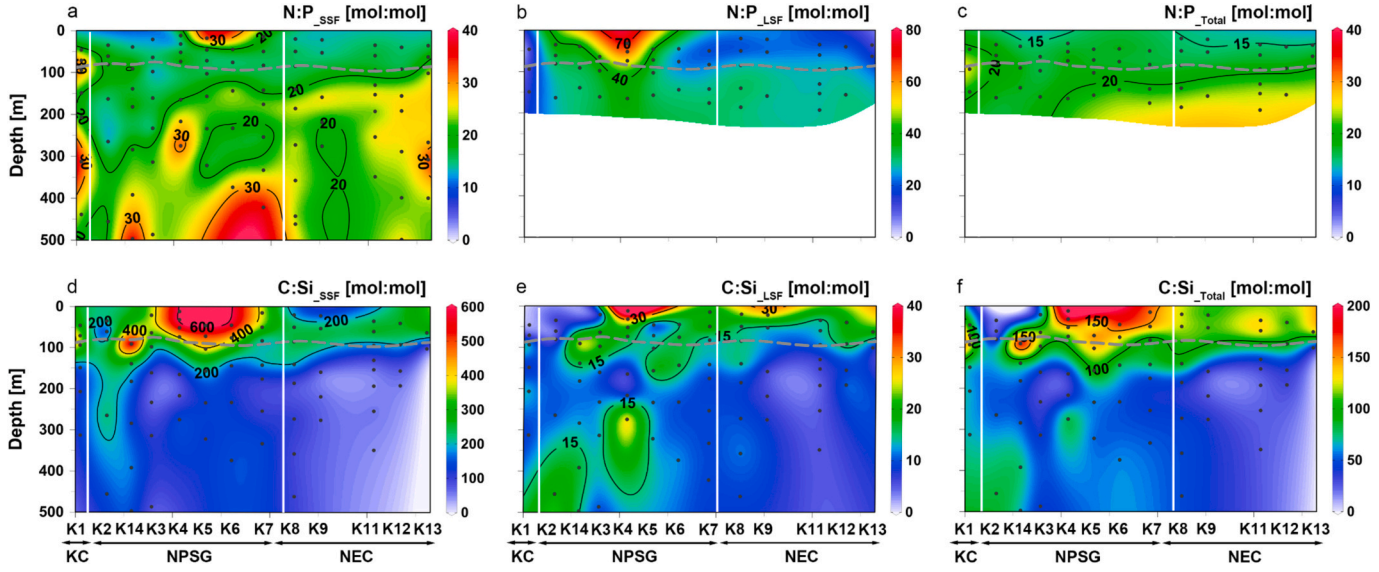

Fig. 5. Distribution of particulate ratios (a-c) N:P and (d-f) C:Si in the upper 500 m of the water column. Left: small size fraction (SSF, 0.8 or 1–51 μm); middle: large size fraction (LSF, >51 μm); right: total particulates (Total, >0.8 or 1 μm). Since particulate P concentrations in the LSF were mostly below the detection limit between 200 and 500 m, $N:P_{LSF}$ and $N:P_{Total}$ ratios in these waters were not calculated. White and gray lines in each panel are depicted in the caption of Fig. 2.

euphotic zone, they decreased rapidly down to 500 m, with an average value of 146 ± 111 mol:mol. In surface water at stations K4 to K6, C:Si_{SSF} ratios were remarkably high, exceeding 600 mol:mol, and corresponding to the highest POC_{SSF} concentration. Vertical distribution patterns of C:Si_{LSF} were generally similar to those of C:Si_{SSF}, with the former ratios consistently lower than the latter. The average C:Si_{LSF} ratio was 17 ± 11 mol:mol in the euphotic zone and 12 ± 6 mol:mol in waters below (Fig. 5e). However, C:Si_{LSF} ratios were extremely low above 100 m and notably high between 400 and 500 m at stations K1 and K2. This pattern was not observed for C:Si_{SSF} (Fig. 5d and e). The C:Si_{Total} ratio showed high values in the euphotic zone (on average 121 ± 50 mol:mol) and gradually decreased with increasing depth (averaging 53 ± 30 mol:mol below the euphotic zone), except for stations K1 and K14, where C:Si_{Total} ratios were consistently higher than 60 from the surface down to 500 m (Fig. 5f). Particulate molar C:Si_{Total} ratios were overall higher than the molar ratio of POC to BSi for cultured diatoms (mostly between 6.6 and 10 mol:mol; Brzezinski, 1985), thus suggesting only a small contribution of diatoms to the phytoplankton biomass of the subtropical wNP.

3.3. Phytoplankton community composition in the euphotic zone

Pigment concentrations of total particles (>0.7 μm) were collected using Niskin bottles during the same cruise, and the relative contribution of major phytoplankters was calculated using the CHEMTAX approach (Browning et al., 2022; Zhang et al., 2024b). The phytoplankton community composition in the euphotic zone at stations K1, K6, and K8, representing the KC, NPSG, and NEC zones, was highly consistent (Fig. 6). Picophytoplankters *Prochlorococcus* and *Synechococcus* (<2 μm in size) together contributed to ~ 80 % of the total Chl-*a* in the euphotic zone. Nanophytoplankter haptophytes_8 (2–20 μm in size), the third major phytoplankton group in all three zones, accounted for ~ 13 % of the total Chl-*a*. Other identified pico- and nanophytoplankters, including prasinophytes, dinoflagellates, chlorophytes, and cryptophytes, collectively contributed to ~ 5 % of the total Chl-*a*. Microphytoplankter diatoms (>20 μm in size), though detected, accounted for only ~ 1 % of the total Chl-*a* in the euphotic zone of the oligotrophic subtropical wNP. Therefore, pigment concentrations of total particles collected by Niskin bottles (>0.7 μm) mainly reflected the phytoplankton community composition in the SSF (0.8 or 1–51 μm) rather than in the LSF (>51 μm).

4. Discussion

4.1. Factors affecting particulate molar C:N:P:Si ratios in the euphotic zone

4.1.1. Small vs. large size fraction

The range of C:N, C:P, and N:P ratios was larger in the LSF than in the SSF in the euphotic zone in the subtropical wNP. There were also significant differences in the average ratio between these two fractions (two-tailed Student's *t*-test, *P* value <0.01). Average C:N, C:P, and N:P ratios were notably higher for the large than the small size fraction, in particular average C:P_{LSF} and N:P_{LSF} ratios were nearly twice those of C:P_{SSF} and N:P_{SSF}. Moreover, both SSF and LSF elemental stoichiometry deviated from the Redfield ratio (Fig. 7a-c).

Considering that *Prochlorococcus* and *Synechococcus* were the major contributors to the phytoplankton biomass in the euphotic zone (Fig. 6), the agreement between C:N, C:P, and N:P ratios in the SSF and those of cultured *Prochlorococcus* and *Synechococcus* (Fig. 7a-c) documents that the SSF primarily represented particles resulting from phytoplankton primary production. On the other hand, C:N, C:P, and N:P ratios in the LSF were higher than those of cultured eukaryotes including microplankton such as diatoms (Fig. 7d). We thus speculate that in addition to diatoms, the LSF might contain other particulate phases altering the elemental stoichiometry, which were likely aggregates of phytodetritus, grazer components, and fecal pellets undergoing remineralization and/or degradation (Minor et al., 1998; Liefer et al., 2024). However, the LSF particle composition, largely unknown in the present study, requires further identification. Given the preferential remineralization of P in organic matter relative to N (Garber, 1984; Anderson and Sarmiento, 1994), followed by the relatively slow degradation of C (Gordon, 1971), LSF can thus be characterized by a surplus of C relative to N and P (Knauer et al., 1979; Frigstad et al., 2011), resulting in elevated C:N, C:P, and N:P ratios. Additionally, since the contribution of LSF to the total pool of POC, PN, and PP was minor (Figs. 2 and 3), both the range and average values of C:N:P ratios for total particulates were generally consistent with those obtained for the SSF (Fig. 7a-c).

In contrast, the average C:Si ratio of the SSF was clearly higher than that of the LSF (Fig. 7d). This is likely because BSi is mostly found in the LSF, while POC predominates in the SSF (Lam et al., 2018; Subhas et al., 2023). Furthermore, the range of C:Si_{Total} ratios was not very close to that of either C:Si_{SSF} or C:Si_{LSF} ratios, suggesting comparable contributions from these two size fractions to the total inorganic "hard part" pool of biogenic opal. Consequently, we analyze factors affecting the variation of total particulate C:N:P ratios and specific size-fractionated C:Si ratios in the euphotic zone, followed by a comparison of these ratios among KC, NPSG, and NEC zones in the subtropical wNP.

4.1.2. Effects of phytoplankton community composition

Variations in particulate C:N:P:Si ratios are associated with a number of factors, such as phytoplankton species composition (Quigg et al., 2003; Martiny et al., 2013a), nutrient supply ratio (Rhee, 1978; Bates et al., 2005), and environmental acclimation (Lomas et al., 2021). Among them, phytoplankton diversity plays a primary role in determining changes in the elemental ratio of the particulates produced (Lomas et al., 2021).

Particulate C:N_{Total} ratios in the euphotic zone were within errors consistent with cellular C:N ratios of *Prochlorococcus*, *Synechococcus*, and eukaryotes (Cuhel and Waterbury, 1984; Brzezinski, 1985; Burkhardt

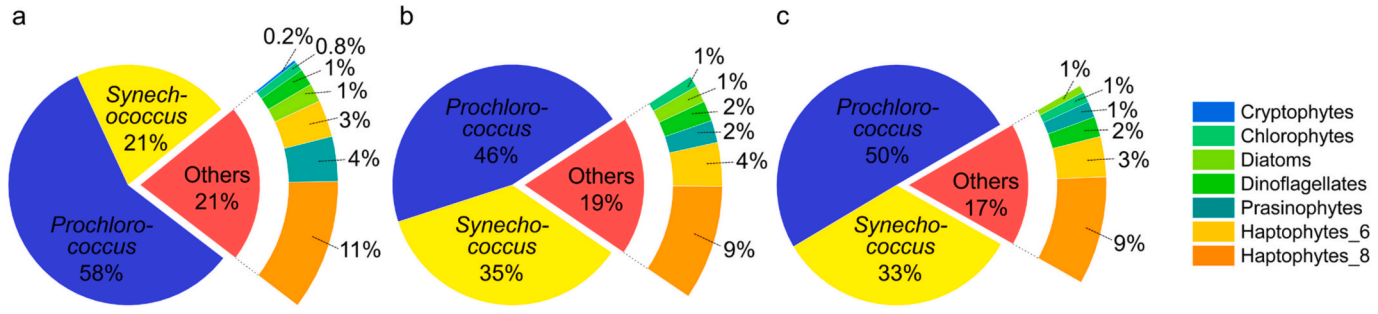

Fig. 6. Phytoplankton community composition in the euphotic zone at stations (a) K1, (b) K6, and (c) K8 representing the Kuroshio Current, North Pacific Subtropical Gyre, and North Equatorial Current zone, respectively. Depth-integrated pigment concentrations of Niskin bottle samples, previously published in Zhang et al. (2024b), were used to calculate the relative contribution of various phytoplankters to the total chlorophyll-*a* in the euphotic zone.

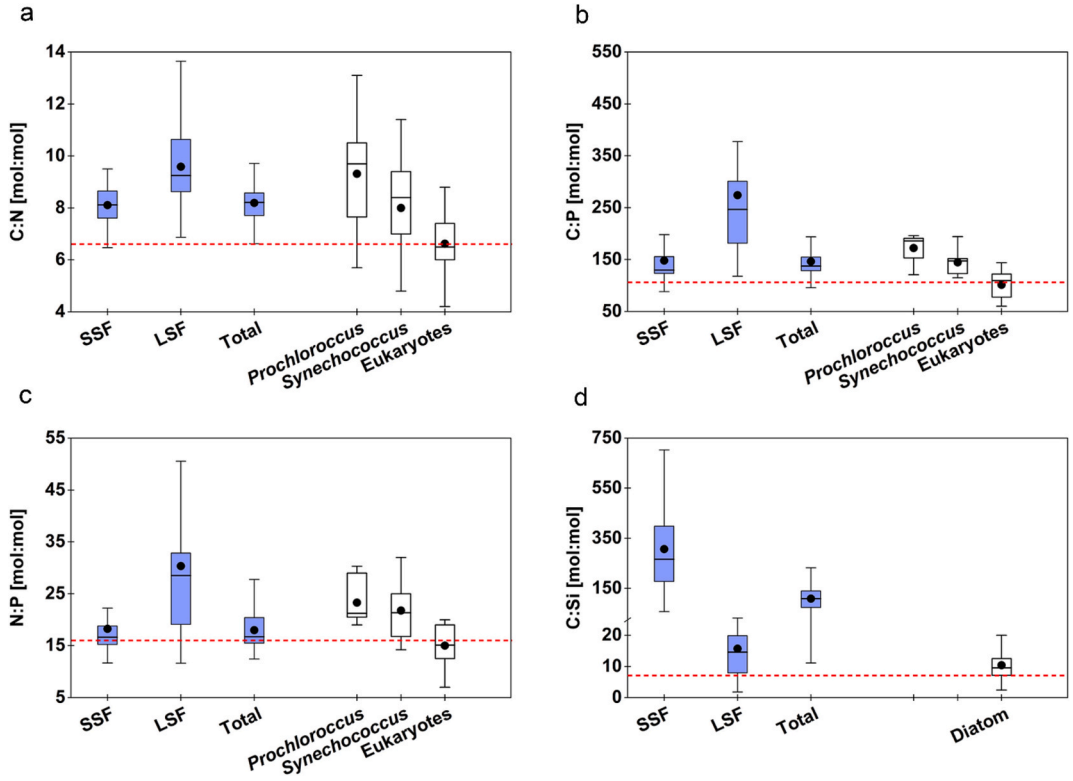

Fig. 7. Box-Whisker plots of (a) C:N, (b) C:P, (c) N:P, and (d) C:Si ratios for the small size fraction (SSF, 0.8 or 1–51 μm), large size fraction (LSF, >51 μm), and total particulates (Total, >0.8 or 1 μm) in the euphotic zone in the subtropical western North Pacific. Cellular stoichiometric ratios of C:N, C:P, and N:P for *Prochlorococcus*, *Synechococcus*, and eukaryotes, and of C:Si for diatoms are shown in open boxes (Cuhel and Waterbury, 1984; Brzezinski, 1985; Burkhardt et al., 1999; Bertilsson et al., 2003; Heldal et al., 2003; Garcia et al., 2016; Martiny et al., 2016; Lomas et al., 2021). Red dashed lines indicate the canonical Redfield ratio values, namely 6.6, 106, and 16 mol:mol for C:N, C:P, and N:P, respectively (Redfield, 1934), as well as the Brzezinski C:Si ratio of 7.1 mol:mol (Brzezinski, 1985). The box defines the 25 % and 75 % quartiles, and the error bars represent the 5 % and 95 % distribution limits. The horizontal line through the box indicates the median value and the black dot in the box represents the average value. (For interpretation of the references to colour in this figure legend, the reader is referred to the web version of this article.)

et al., 1999; Bertilsson et al., 2003; Heldal et al., 2003; Garcia et al., 2016; Martiny et al., 2016; Lomas et al., 2021), whereas some high values exceeded the range of ratios characteristic of eukaryotes (Fig. 7a). The average particulate C:N$_{Total}$ ratio (8.0 mol:mol) obtained in the subtropical wNP coincided with that of *Synechococcus* (8.0 mol:mol) and was slightly lower and higher than that of *Prochlorococcus* (9.3 mol:mol) and eukaryotes (6.6 mol:mol), respectively, indicating a major signature contribution by these three species/groups. This finding is consistent with the pigment analysis of samples collected during the same cruise (Fig. 6). It is noteworthy that the average C:N$_{Total}$ ratio obtained in the present study was slightly higher than the global ocean average reported by Martiny et al. (2013b) and fell within the range of C:N values determined for the entire subtropical North Pacific (3.5–14.2 mol:mol; Talmy et al., 2016; Zhang et al., 2024a).

Particulate C:P$_{Total}$ ratios in the euphotic zone were within errors consistent with cellular C:P ratios of both *Prochlorococcus* and *Synechococcus*, whereas most values exceeded the range of eukaryote ratios (Fig. 7b). The average value (146 mol:mol) fell between that of the former two phytoplankters (172 and 145 mol:mol, respectively) (Fig. 7b), and was consistent with findings in other subtropical regions (Tanioka et al., 2022). However, the majority of C:P$_{Total}$ ratios with a median value of 135 mol:mol exceeded the canonical Redfield C:P ratio, as well as the average value of eukaryotes (102 mol:mol) (Ho et al., 2003; Quigg et al., 2003; Cunningham and John, 2017; Sharoni and Halevy, 2020; Lomas et al., 2021).

Particulate N:P$_{Total}$ ratios in the euphotic zone ranged between 14 and 28 mol:mol and were also within errors comparable to cellular N:P ratios of *Prochlorococcus* and *Synechococcus* (Fig. 7c). The average N:P$_{Total}$ ratio of 17 mol:mol was slightly lower than that of 20 mol:mol for the entire subtropical Pacific (Lomas et al., 2021) and of both *Prochlorococcus* (23 mol:mol) and *Synechococcus* (22 mol:mol) (Cuhel and Waterbury, 1984; Burkhardt et al., 1999; Bertilsson et al., 2003; Heldal et al., 2003; Garcia et al., 2016; Martiny et al., 2016). Nutrient limitation provides one potential explanation for this result. Prior studies indicated that under N limitation, the P cell quota increases in both large- and small-celled phytoplankton taxa, whereas *Prochlorococcus* and *Synechococcus* exhibit a decrease in the N quota (Leonardos and Geider, 2004; Mouginot et al., 2015; Garcia et al., 2016; Moreno and Martiny, 2018; Liefer et al., 2024). In this context, the subtropical wNP, where primary production is mainly N-limited (Wen et al., 2022), tends to show relatively low particulate N:P ratios.

The average particulate C:Si$_{SSF}$ ratio (344 mol:mol) was more than 20 times higher than the average C:Si$_{LSF}$ ratio (17 mol:mol) in the euphotic zone for all sampling stations. This contrast reflects the fact that BSi-rich microplankton (e.g., dinoflagellates and diatoms) were largely collected by 51 μm mesh prefilters, while non-siliceous picophytoplankton were mainly retained on 1 μm-QMA or 0.8 μm-PES filters. Both the range and average value of C:Si$_{Total}$ ratios (120 ± 48 mol:mol) in the euphotic zone in the subtropical wNP were notably higher than the cellular C:Si ratios of cultured diatoms (mostly between 6.6 and 10 mol:mol; Brzezinski, 1985) (Fig. 7d). This deviation further suggests that diatoms accounted for only a minor fraction of the particles larger than 0.8 μm in the oligotrophic subtropical wNP (Browning et al., 2022).

We take a look at the relationship between particulate elemental ratios and pigment proportions in the euphotic zone. There were relatively strong positive correlations between C:P$_{Total}$ and N:P$_{Total}$ ratios

and *Prochlorococcus* proportions, as well as a weak negative correlation between C:N$_{Total}$ ratios and eukaryote proportions (Fig. S2c, d and g). Among *Prochlorococcus*, *Synechococcus*, and eukaryotes, *Prochlorococcus* exhibits the highest cellular C:P and N:P ratios, while eukaryotes generally have lower cellular C:N ratios compared to the other two picophytoplankters (Fig. 7a-c). Consequently, increased *Prochlorococcus* proportions could elevate C:P$_{Total}$ and N:P$_{Total}$ ratios, while increased eukaryote proportions tended to lower C:N$_{Total}$ ratios. These relationships, overall, indicate the primary effect of phytoplankton community composition on elemental ratios of total particles mainly determined by the SSF.

Prior studies suggested that environmental factors play an important role in regulating the elemental stoichiometry of marine particles (Moreno and Martiny, 2018; Tanioka and Matsumoto, 2020; Lomas et al., 2021; Zhang et al., 2024a). We analyze the relationship between total particulate C:N:P:Si ratios and temperature, light intensity, and nutrient concentrations in the euphotic zone in the subtropical wNP. Although the results indicate no significant correlation between any of these ratios and any of these environment factors during the sampling period (all P values >0.05; Fig. S3), the environmental effect on particulate elemental ratios cannot be ruled out. The absence of significant correlations might be simply because the environmental factors displayed relatively small variations in the investigated region. In contrast, Tanioka and Matsumoto (2020) examined these relationships based on a number of laboratory culture experiments with notable variations in environmental conditions and found significant correlations (P values <0.05). We contend that despite the relatively small variation in environmental conditions in our research domain, they may have impacted particulate elemental ratios mainly by shaping the phytoplankton community composition in the euphotic zone.

4.1.3. KC and NPSG zones vs. NEC zone

The elemental stoichiometry of total particles in the euphotic zone was comparable between KC plus NPSG (stations K1 to K7 and K14) and NEC zones (stations K8 to K13) (Fig. 8a). However, average C:P$_{Total}$ and N:P$_{Total}$ ratios were significantly higher in the KC and NPSG zones than in the NEC zone (two-tailed Student's t-test, P value <0.05), corresponding to higher N_2 fixation rates in the former than in the latter (Wen et al., 2022). It is noteworthy that overall lower $\delta^{15}N_{PN}$ signatures were determined at stations K1 to K7 and K14 (−2.8 to 2.6 ‰) than at stations K8 to K13 (1.4 to 5.2 ‰) (Fig. 8b and c), pointing to potential differences in the influence of N_2 fixation among these zones.

Dinitrogen fixation has been found to be a major factor responsible for elevated elemental ratios of C:N (Fulweiler, 2023), C:P (Follett et al., 2018), and N:P (Follett et al., 2018) in biogenic particles. Laboratory culture experiments have also demonstrated a strong positive correlation between particulate C:P and N:P ratios and N_2 fixation rates (Follett et al., 2018). Future investigations based on both field observations and incubation experiments are needed to explore the potential impact of N_2 fixation on particulate C:N:P ratios.

Higher N_2 fixation in the KC and NPSG zones could produce relatively abundant nutrients such as ammonia in the euphotic zone, which can be utilized by non-siliceous phytoplankton and result in an increased C quota (Wang et al., 2019) likely contributing to the higher (by 40 %) C:Si ratios in the KC plus NPSG compared to the NEC zone. However, the negligible difference in C:Si$_{Total}$ ratios among these zones (Fig. 8a) may be ascribed to the fact that diatoms are not the dominant phytoplankton taxon in the entire research domain (Browning et al., 2022; Yuan et al., 2023).

4.2. Factors affecting particulate molar C:N:P:Si ratios below the euphotic zone

4.2.1. Particulate molar C:N:P ratios

Since SSF was the dominant contributor to the total particulate C:N, C:P, and N:P ratios (Fig. 7), we discuss the vertical distribution of C:N$_{SSF}$, C:P$_{SSF}$, and N:P$_{SSF}$ between the euphotic zone bottom and 500 m. In contrast to the results obtained in the euphotic zone, C:N$_{SSF}$, C:P$_{SSF}$, and N:P$_{SSF}$ ratios in waters below tended to generally increase with depth (Fig. 9a-c). Prior studies also showed elevated stoichiometric ratios of these particulate elements with increasing depth below the euphotic zone (Schneider et al., 2003; Xu et al., 2021). This gradient probably occurs because remineralization or degradation rates vary among different bioelements. Proteins and phospholipids rich in N or P are preferentially remineralized, whereas carbohydrates are remineralized more slowly. Consequently, P is preferentially lost relative to N and C during organic matter degradation (Shaffer et al., 1999; Slomp et al., 2004; Letscher and Moore, 2015; Matsumoto et al., 2020a), leading to increasing C:N$_{SSF}$, C:P$_{SSF}$, and N:P$_{SSF}$ ratios with depth below the euphotic zone.

4.2.2. Particulate molar C:Si ratio

Since both SSF and LSF essentially contributed to the total particulate C:Si ratio (Fig. 5d-f), we discuss the vertical distribution of C:Si$_{Total}$ ratios below the euphotic zone. Differing from C:N:P ratios, C:Si$_{Total}$ ratios initially decreased and subsequently remained relatively constant from the euphotic zone bottom to 500 m (Fig. 9d), which is due to the fact that POC concentrations usually peak in surface water and decrease with depth, whereas the maximum BSi concentration often occurs in the deep chlorophyll maximum layer (Kemp and Villareal, 2013; Tréguer

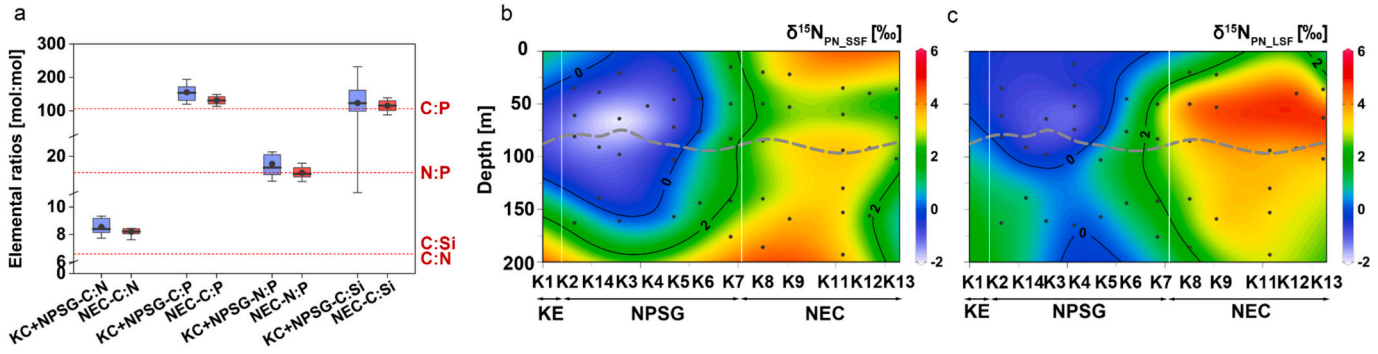

Fig. 8. (a) Box-Whisker plots of C:N:P:Si ratios for total particulates (Total, >0.8 or 1 μm) in the euphotic zone in the Kuroshio Current and North Pacific Subtropical Gyre (KC + NPSG) (blue boxes) and in the North Equatorial Current (NEC; red boxes). Distributions of particulate N stable isotopic composition ($\delta^{15}N_{PN}$) of (b) small size fraction (SSF, 1–51 μm) and (c) large size fraction (LSF, >51 μm) in the upper 200 m of the water column. In panel (a), the red dashed lines and Box-Whisker features are defined in the caption of Fig. 7. The canonical C:Si and C:N ratios are hardly discriminated with the selected scale for the y-axis. In panels (b) and (c), white and gray lines are depicted in the caption of Fig. 2. (For interpretation of the references to colour in this figure legend, the reader is referred to the web version of this article.)

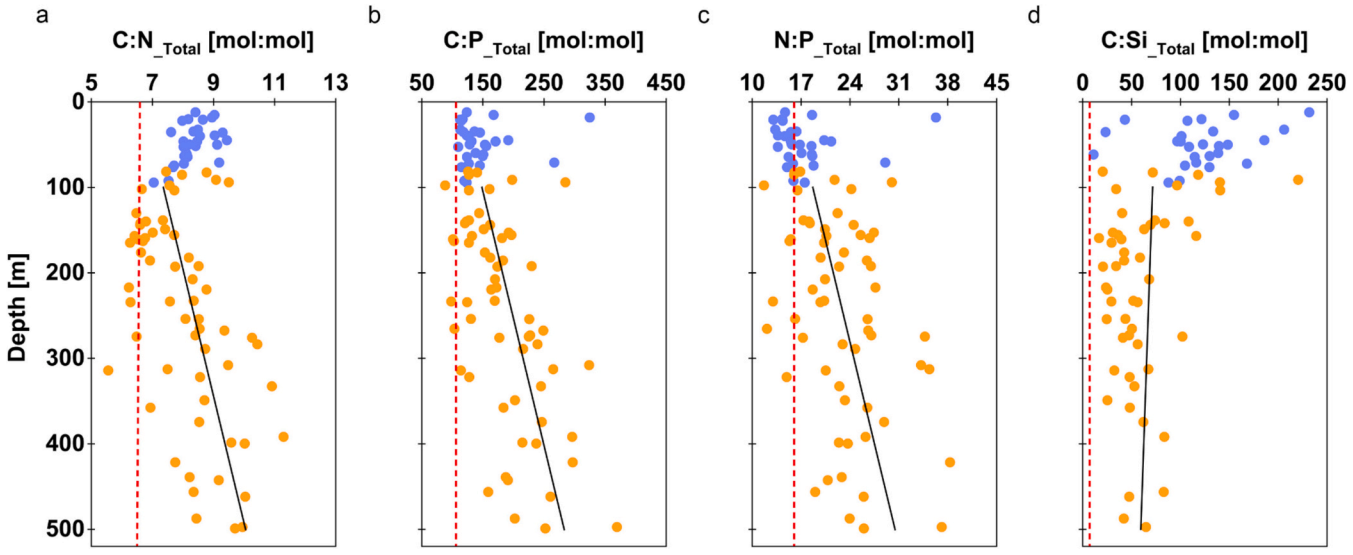

Fig. 9. Vertical distributions of (a) $C:N_{\_SSF}$, (b) $C:P_{\_SSF}$, (c) $N:P_{\_SSF}$, and (d) $C:Si_{\_Total}$ ratios in the upper 500 m of the water column at all sampling stations. Blue and yellow circles denote data collected in and below the euphotic zone, respectively. In each panel, black solid lines depict the distribution trend of each ratio with increasing depth below the euphotic zone, while red dashed lines indicate the canonical Redfield ratio values, namely 6.6, 106, and 16 mol:mol for C:N, C:P, and N:P, respectively (Redfield, 1934), as well as the Brzezinski C:Si ratio of 7.1 mol:mol (Brzezinski, 1985). (For interpretation of the references to colour in this figure legend, the reader is referred to the web version of this article.)

et al., 2018). Both POC and BSi concentrations were relatively low below the euphotic zone, with slow remineralization or dissolution rate (Liu et al., 2019) likely preventing C:Si ratios to increase with depth.

4.2.3. High particulate molar C:P and N:P ratios

Particulate $C:P_{\_SSF}$ and $N:P_{\_SSF}$ ratios exhibited relatively high values at around 300–500 m of stations K2 to K7, K13, and K14 (Figs. 4d and 5a). High N_2 fixation rates have been previously observed in the NPSG zone (Wen et al., 2022), where particulate $C:P_{\_SSF}$ and $N:P_{\_SSF}$ ratios were also elevated in surface water (Figs. 4d and 5a). This coincidence may indicate that high POC and PN relative to PP concentrations, due to extra nutrients resulting from N_2 fixation, could be exported to deep waters (Tanioka et al., 2022). On the other hand, stations K13 and K14 located near the Philippines archipelago exhibited low $\delta^{13}C$ signatures (−24.0 to −25.9 ‰) of POC between 300 and 500 m. This feature suggests a potential influence of terrestrial materials transported by advection and/or horizontal mixing, which may yield elevated $C:P_{\_SSF}$ and $N:P_{\_SSF}$ ratios (Zhang et al., 2021).

4.3. Comparison with the subtropical eastern South Pacific and North Atlantic

We compare data of biogenic particle concentrations (Fig. 10) and particulate C:N:P:Si ratios (Fig. 11) in the euphotic zone in three oceanic settings: the subtropical wNP (GP09 section; data obtained during GEOTRACES-GP09 cruise; this study), the subtropical eSP divided into the open gyre (GP16-O section) and the Peru coastal upwelling and eastern boundary (GP16-C section) (data obtained during GEOTRACES-GP16 cruise; Lam et al., 2018; GEOTRACES Intermediate Data Product Group, 2021), and the subtropical NA divided into the open gyre (GA03-O section) and the southeastern boundary (GA03-C section) (data obtained during GEOTRACES-GA03 cruise; Lam et al., 2015; Bourne et al., 2018; GEOTRACES Intermediate Data Product Group, 2021).

Generally similar to the subtropical wNP, the contribution of the LSF to the total pool of POC, PN, and PP was relatively small in the subtropical eSP and NA. Total biogenic particle concentrations (Fig. 10a-c) and their stoichiometric ratios (Fig. 11a-c) were largely consistent with those for the SSF in the euphotic zone. In contrast, both size fractions made comparable contributions to the total BSi pool, with $C:Si_{\_Total}$ ratios ranging between $C:Si_{\_SSF}$ and $C:Si_{\_LSF}$ ratios (Figs. 10d and 11d).

4.3.1. Biogenic particle concentrations

Both the range and average values of total (SSF + LSF) POC, PN, and PP concentrations in the euphotic zone in the GP16-C section were notably higher than those in the GP16-O, followed by GP09 and GA03 sections. BSi concentrations were notably higher in coastal regions than in open gyres of both the subtropical eSP and NA (Fig. 10d). We attribute these contrasts to differences in primary productivity. Specifically, strong upwelling of nutrient-rich deep waters in the GP16-C section stimulated the highest primary productivity and biogenic particle concentrations among these five sections (Lam et al., 2018; Peters et al., 2018; Grasse et al., 2020).

Total biogenic particle concentrations in the GP16-O section were comparable to or slightly higher than those in the GP09 section (Fig. 10). However, except for POC concentrations (Fig. 10a), both average and median concentrations of other biogenic particles in the euphotic zone in the GP16-O section were consistently higher than those in the GP09 section (two-fold and three-fold higher for $PP_{\_Total}$ and $BSi_{\_Total}$, respectively; Fig. 10b-d). The GP16-O section was located north of the high-productivity region, and was also supplied by nutrients via southward and westward flowing equatorial waters (Kessler, 2006; Peters et al., 2018). This could at least partly explain the somewhat higher PN, PP, and BSi concentrations in the GP16-O section relative to those in the GP09 section.

Both GA03-O and GP09 sections were located in the oligotrophic gyre, where biological productivity is extremely low (Dai et al., 2023). The average concentration of various biogenic particles was thus at a low level and generally agreed well between these two sections (Fig. 10). BSi concentrations were notably high in the GA03-C section compared to in GA03-O and GP09 sections. High dust deposition fluxes into the eastern boundary of the subtropical NA (Shelley et al., 2015) might serve as an important external source of nutrients in seawater stimulating diatom growth.

4.3.2. Particulate molar C:N:P:Si ratios

The highest average $C:N_{\_Total}$ and $N:P_{\_Total}$ ratios in the euphotic zone were observed in the GP09 section, both of which were comparable to the cellular elemental stoichiometric ratios of *Prochlorococcus* and

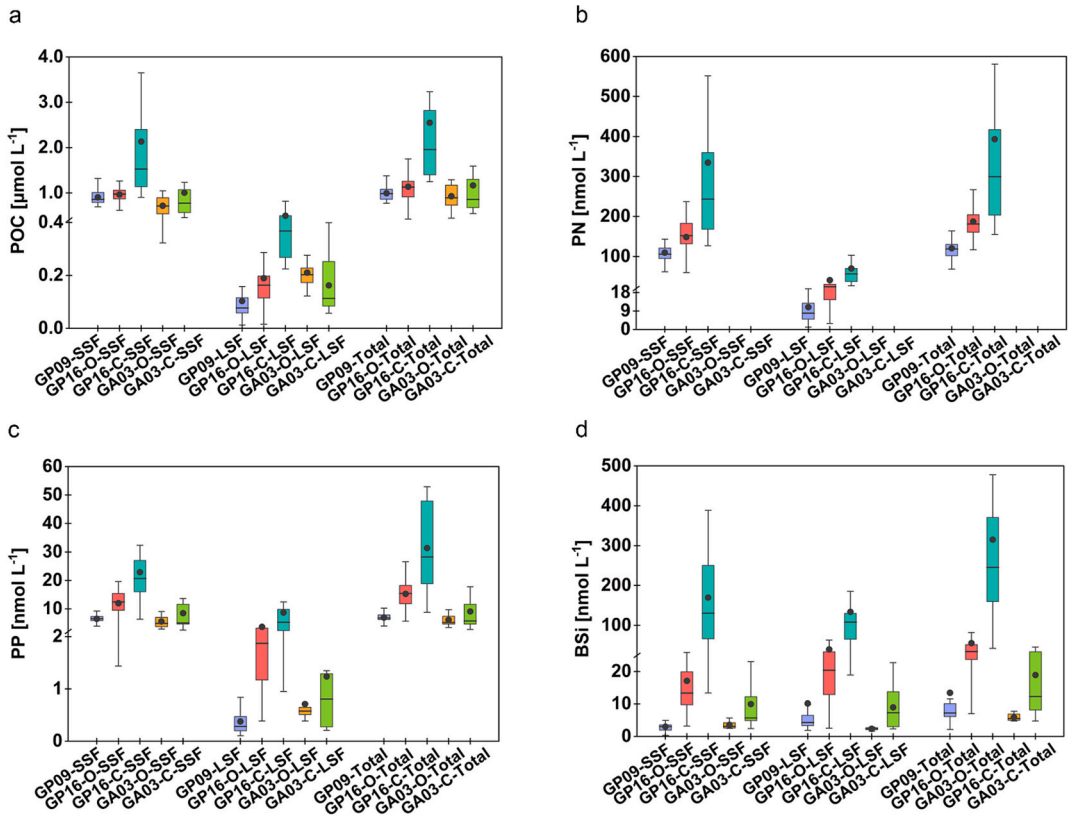

Fig. 10. Box-Whisker plots of (a) particulate organic carbon, POC, (b) particulate nitrogen, PN, (c) particulate phosphorus, PP, and (d) biogenic silica, BSi concentrations, for the small size fraction (SSF, 0.8 or 1–51 μm), large size fraction (LSF, >51 μm), and total particulates (Total, >0.8 or 1 μm) in the euphotic zone in the subtropical western North Pacific (blue boxes, data obtained during the GEOTRACES-GP09 cruise; this study), the subtropical eastern South Pacific gyre (red boxes, data obtained in the open ocean region during GEOTRACES-GP16 cruise (GP16-O); Lam et al., 2018), the Peru coastal upwelling and eastern boundary (dark green boxes, data obtained in the coastal region during the GEOTRACES-GP16 cruise (GP16-C); Lam et al., 2018; GEOTRACES Intermediate Data Product Group, 2021), the subtropical North Atlantic gyre (orange boxes, data obtained in the open ocean region during GEOTRACES-GA03 cruise (GA03-O); Lam et al., 2015; Bourne et al., 2018; GEOTRACES Intermediate Data Product Group, 2021), and the southeastern boundary of the subtropical North Atlantic (brilliant green boxes, data obtained in the coastal region during GEOTRACES-GA03 cruise (GA03-C); Lam et al., 2015; Bourne et al., 2018; GEOTRACES Intermediate Data Product Group, 2021). The Box-Whisker features in each panel are defined in the caption of Fig. 7. (For interpretation of the references to colour in this figure legend, the reader is referred to the web version of this article.)

Synechococcus and were higher than the Redfield ratio (Fig. 11a and c). C:$P_{\_Total}$ ratios in the euphotic zone in GP09 and GA03 sections were overall comparable and together higher than those in GP16 sections (Fig. 11b).

Lam et al. (2018) found a strong correlation between PP and particulate Fe concentrations in the hydrothermal plume, and attributed lower C:P ratios in GP16 sections to the potentially high contribution of hydrothermal-sourced PP. On the other hand, picophytoplankters dominate the phytoplankton community in both the subtropical wNP and NA (Twining et al., 2015; Browning et al., 2022; Zhang et al., 2024b). Correspondingly, C:$P_{\_Total}$ ratios in the euphotic zone in GP09 and GA03 sections were within errors comparable with the cellular C:P ratios of *Prochlorococcus* and *Synechococcus*. However, both the range and average of C:$P_{\_Total}$ ratios in GP16-O and GP16-C sections were roughly equal or only slightly lower than the cellular C:P and N:P ratios of eukaryotes (Fig. 11b). This result indicates that the composition of the phytoplankton community may be another important factor influencing particulate C:N:P ratios (Ohnemus et al., 2017; Browning et al., 2022).

The range of particulate C:Si ratios in GP09 and GA03-O sections were comparable to that in GP16-O and GA03-C sections, although the average value in the former section was slightly higher than that in the latter, and both were markedly higher than the cellular C:Si ratios of diatoms (Brzezinski, 1985). In contrast, both the range and average of the particulate C:Si ratios in the GP16-C section aligned with the cellular C:Si ratios of diatoms (Fig. 11d). This result is again consistent with pigment analysis which showed that diatoms dominated the phytoplankton community in the upper water column of the GP16-C section (Ohnemus et al., 2017). The above finding further suggests that the composition of the phytoplankton assemblage plays an important role in determining the variation in particulate elemental ratios.

In the euphotic zone, the lowest C:$P_{\_Total}$ and N:$P_{\_Total}$ ratios in the GP09 section, as well as the lowest C:$P_{\_Total}$ ratio in the GA03-O section, were roughly consistent with the canonical Redfield ratio. Moreover, the lowest C:$Si_{\_Total}$ ratio in the GP16-C section was nearly identical to the canonical Brzezinski ratio (Fig. 11). The former particulate C:N:P ratios aligned well with those of *Prochlorococcus* and *Synechococcus*, the dominant phytoplankters in GP09 and GA03-O sections; the latter particulate C:Si ratio matched that of diatoms, the dominant phytoplankter in the GP16-C section. These consistencies tend to suggest that in some circumstances, the phytoplankton community composition could set a lower bound of particulate C:N:P:Si ratios, while specific mechanisms require further examinations.

5. Conclusions and Implications

Biogenic particle concentrations and particulate C:N:P:Si ratios showed noticeable spatial variations and distinct differences between size fractions in the upper 500 m of the subtropical wNP. The average concentrations of POC, PN, and PP in the SSF were an order of magnitude higher than those in the LSF, whereas the average BSi

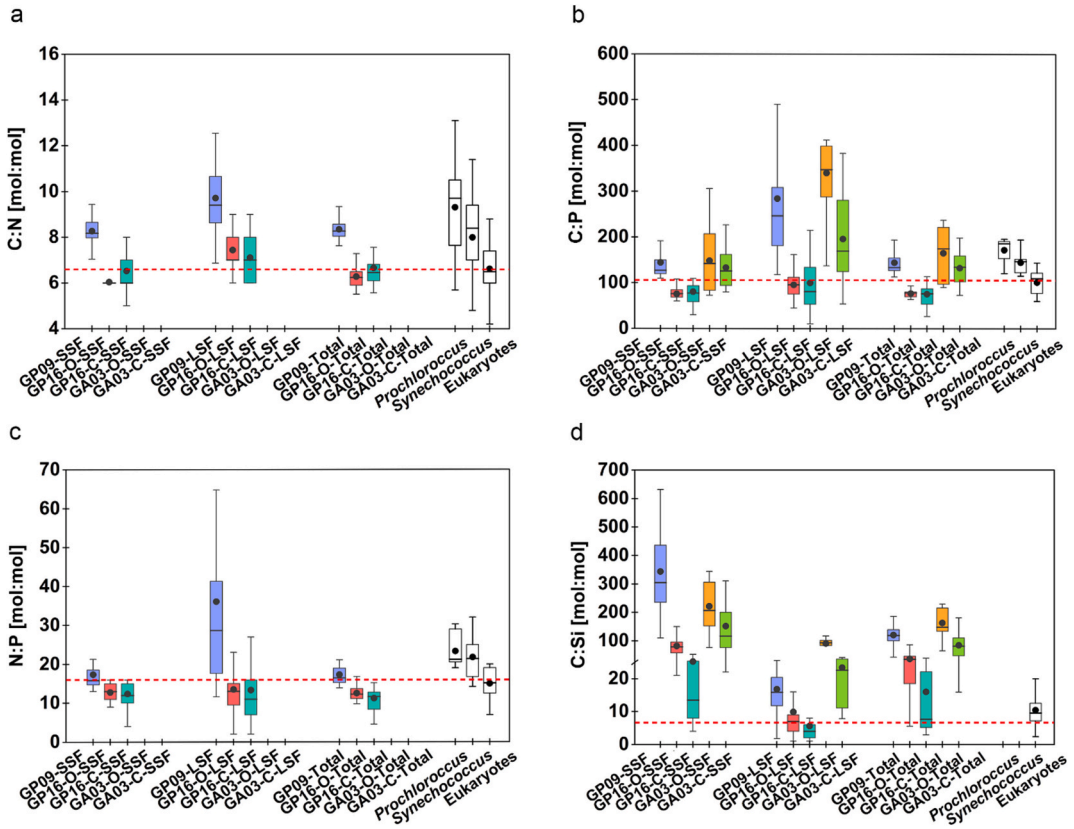

Fig. 11. Box-Whisker plots of (a) C:N, (b) C:P, (c) N:P, and (d) C:Si ratios for the small size fraction (SSF, 0.8 or 1–51 μm), large size fraction (LSF, >51 μm), and total particulates (Total, >0.8 or 1 μm) in the euphotic zone in the subtropical western North Pacific (blue boxes, data obtained during the GEOTRACES-GP09 cruise; this study), the subtropical eastern South Pacific gyre (red boxes, data obtained in the open ocean region during GEOTRACES-GP16 cruise (GP16-O); Lam et al., 2018), the Peru coastal upwelling and eastern boundary (dark green boxes, data obtained in the coastal region during the GEOTRACES-GP16 cruise (GP16-C); Lam et al., 2018; GEOTRACES Intermediate Data Product Group, 2021), the subtropical North Atlantic gyre (orange boxes, data obtained in the open ocean region during GEOTRACES-GA03 cruise (GA03-O); Lam et al., 2015; Bourne et al., 2018; GEOTRACES Intermediate Data Product Group, 2021), and the southeastern boundary of the subtropical North Atlantic (brilliant green boxes, data obtained in the coastal region during GEOTRACES-GA03 cruise (GA03-C); Lam et al., 2015; Bourne et al., 2018; GEOTRACES Intermediate Data Product Group, 2021). Cellular stoichiometric ratios C:N, C:P, and N:P for *Prochlorococcus*, *Synechococcus*, and eukaryotes, and C:Si for diatoms are shown in open boxes (Cuhel and Waterbury, 1984; Brzezinski, 1985; Burkhardt et al., 1999; Bertilsson et al., 2003; Heldal et al., 2003; Garcia et al., 2016; Martiny et al., 2016; Lomas et al., 2021). The red dashed lines and Box-Whisker features in each panel are defined in the caption of Fig. 7. (For interpretation of the references to colour in this figure legend, the reader is referred to the web version of this article.)

concentration was generally higher in the LSF compared to the SSF. The LSF exhibited higher particulate molar C:N, C:P, and N:P ratios, but lower particulate molar C:Si ratios. Due to the major contribution of the SSF to the total POC, PN, and PP pool, the distribution pattern and range of C:N:P$_{_Total}$ ratios resembled those of the SSF, whereas C:Si$_{_Total}$ values ranged between C:Si$_{_SSF}$ and C:Si$_{_LSF}$ values. In the euphotic zone, the phytoplankton community composition primarily controlled the elemental ratio of the SSF and total particles. Below the euphotic zone, particulate molar C:N$_{_SSF}$, C:P$_{_SSF}$, and N:P$_{_SSF}$ ratios all increased with depth but at different rates down to 500 m, presumably due to the preferential remineralization of P and N compared to C.

Complementing the global analysis of Martiny et al. (2013a), our results reveal latitudinal gradients of particulate C:N:P:Si ratios at a regional scale. These ratios were higher in KC and NPSG zones than in the southern NEC zone, and suggest a primary control by the composition of the phytoplankton community. Moreover, our findings suggest that N_2 fixation could lead to an increase in particulate C:P ratios, as a given portion of P can promote a larger portion of C assimilation. While oligotrophic gyres are projected to expand under global warming (Polovina et al., 2008; Lomas et al., 2021), increases in N_2 fixation rates (Dai et al., 2023) and subsequent enhancement in P utilization efficiency (Follett et al., 2018) may help sustain or increase rates of oceanic C fixation and export from surface to deep waters in these gyres.

CRediT authorship contribution statement

Chaoyong Wang: Writing – original draft, Software, Formal analysis. **Kan Zhang:** Writing – review & editing, Methodology. **Zhimian Cao:** Writing – review & editing, Validation, Supervision, Project administration, Funding acquisition. **Kuanbo Zhou:** Writing – review & editing, Supervision. **Zhongwei Yuan:** Writing – review & editing. **Junhui Chen:** Methodology. **Yifan Ma:** Methodology. **Bei Zhou:** Methodology. **Xin Liu:** Methodology. **Yihua Cai:** Investigation. **Dalin Shi:** Writing – review & editing. **Minhan Dai:** Writing – review & editing, Project administration, Funding acquisition.

Declaration of Competing Interest

The authors declare that they have no known competing financial interests or personal relationships that could have appeared to influence the work reported in this paper.

Acknowledgements

This study was funded by the National Natural Science Foundation of China (92258302) and the National Key Research and Development Plan (2023YFF0805001) sponsored by the Ministry of Science and Technology of China. Chaoyong Wang was supported by the Xiamen

University Nanqiang Cultivation Program for Outstanding Doctoral Students. We thank Yating Li, Feipeng Xu, Liguo Guo, Lifang Wang, Tao Huang, Yanping Xu, Yuanchen Li, Jinping Yu, and Ming Xu for their assistance in sampling and/or analysis. We are grateful to the GEOTRACE-GP09 cruise and the captain, crew, and scientists of the R/V *Tan Kah Kee* for their help during the cruise. Constructive comments by Katsumi Matsumoto and an anonymous reviewer greatly improved the quality of this contribution.

Appendix A. Supplementary data

Supplementary data to this article can be found online at https://doi.org/10.1016/j.gloplacha.2025.104732.

Data availability

Data will be made available on request.

References

Alexander, H., Jenkins, B.D., Rynearson, T.A., Dyhrman, S.T., 2015. Metatranscriptome analyses indicate resource partitioning between diatoms in the field. Proc. Natl. Acad. Sci. USA 112, E2182–E2190. https://doi.org/10.1073/pnas.1421993112.

Anderson, L.A., Sarmiento, J.L., 1994. Redfield ratios of remineralization determined by nutrient data analysis. Glob. Biogeochem. Cycles 8, 65–80. https://doi.org/10.1029/93GB03318.

Arrigo, K.R., Dunbar, R.B., Lizotte, M.P., Robinson, D., 2002. Taxon-specific differences in C/P and N/P drawdown for phytoplankton in the Ross Sea, Antarctica. Geophys. Res. Lett. 29, 1938. https://doi.org/10.1029/2002GL015277.

Baer, S.E., Lomas, M.W., Terpis, K.X., Mouginot, C., Martiny, A.C., 2017. Stoichiometry of *Prochlorococcus*, *Synechococcus*, and small eukaryotic populations in the western North Atlantic Ocean. Environ. Microbiol. 19, 1568–1583. https://doi.org/10.1111/1462-2920.13672.

Bates, N.R., Hansell, D.A., Moran, S.B., Codispoti, L.A., 2005. Seasonal and spatial distribution of particulate organic matter (POM) in the Chukchi and Beaufort Seas. Deep Sea Res. Part II Top. Stud. Oceanogr. 52, 3324–3343. https://doi.org/10.1016/j.dsr2.2005.10.003.

Bertilsson, S., Berglund, O., Karl, D.M., Chisholm, S.W., 2003. Elemental composition of marine *Prochlorococcus* and *Synechococcus*: Implications for the ecological stoichiometry of the sea. Limnol. Oceanogr. 48, 1721–1731. https://doi.org/10.4319/lo.2003.48.5.1721.

Bonachela, J., Allison, S., Martiny, A., Levin, S.A., 2013. A model for variable phytoplankton stoichiometry based on cell protein regulation. Biogeosciences 10, 4341–4356. https://doi.org/10.5194/bg-10-4341-2013.

Bourne, H.L., Bishop, J.K.B., Lam, P.J., Ohnemus, D.C., 2018. Global spatialand temporal variation of Cd:P in euphotic zone particulates. Glob. Biogeochem. Cycles 32, 1123–1141. https://doi.org/10.1029/2017GB005842.

Broecker, W.S., Peng, T.H., 1982. Tracers in the Sea. In: Lamont Doherty Earth Observatory. Columbia University, Palisades, New York. https://doi.org/10.1017/S0033822200005221.

Browning, T.J., Liu, X., Zhang, R., Wen, Z., Liu, J., Zhou, Y., Xu, F., Cai, Y., Zhou, K., Cao, Z., Zhu, Y., Shi, D., Achterberg, E., Dai, M., 2022. Nutrient co-limitation in the subtropical Northwest Pacific. Limnol. Oceanogr. Lett. 7, 52–61. https://doi.org/10.1002/lol2.10205.

Brzezinski, M.A., 1985. The Si:C:N ratio of marine diatoms: interspecific variability and the effect of some environmental variables. J. Phycol. 21, 347–357. https://doi.org/10.1111/j.0022-3646.1985.00347.x.

Brzezinski, M.A., Krause, J.W., Church, M.J., Karl, D.M., Li, B., Jones, J.L., Updyke, B., 2011. The annual silica cycle of the North Pacific subtropical gyre. Deep Sea Res. I: Oceanogr. Res. Pap. 58, 988–1001. https://doi.org/10.1016/j.dsr.2011.08.001.

Burkhardt, S., Zondervan, I., Riebesell, U., 1999. Effect of CO_2 concentration on C:N:P ratio in marine phytoplankton: a species comparison. Limnol. Oceanogr. 44, 683–690. https://doi.org/10.4319/lo.1999.44.3.0683.

Cao, Z., Wang, D., Zhang, Z., Zhou, K., Liu, X., Wang, L., Huang, B., Cai, P., Dai, M., 2020. Seasonal dynamics and export of biogenic silica in the upper water column of a large marginal sea, the northern South China Sea. Prog. Oceanogr. 188, 102421. https://doi.org/10.1016/j.pocean.2020.102421.

Chow, C.H., Cheah, W., Tai, J.H., Liu, S.F., 2019. Anomalous wind triggered the largest phytoplankton bloom in the oligotrophic North Pacific Subtropical Gyre. Sci. Rep. 9, 15550. https://doi.org/10.1038/s41598-019-51989-x.

Cuhel, R.L., Waterbury, J.B., 1984. Biochemical composition and short term nutrient incorporation patterns in a unicellular marine cyanobacterium, *Synechococcus* (WH7803). Limnol. Oceanogr. 29, 370–374. https://doi.org/10.4319/lo.1984.29.2.0370.

Cunningham, B.R., John, S.G., 2017. The effect of iron limitation on cyanobacteria major nutrient and trace element stoichiometry. Limnol. Oceangor. 62, 846–858. https://doi.org/10.1002/lno.10484.

Dai, M., Luo, Y.W., Achterberg, E.P., Browning, T.J., Cai, Y., Cao, Z., Chai, F., Chen, B., Church, M.J., Ci, D., Du, C., Gao, K., Guo, X., Hu, Z., Kao, S.J., Laws, E.A., Lee, Z., Lin, H., Liu, Q., Liu, X., Luo, W., Meng, F., Shang, S., Shi, D., Saito, H., Song, L., Wan, X.S., Wang, Y., Wang, W.L., Wen, Z., Xiu, P., Zhang, J., Zhang, R., Zhou, K., 2023. Upper ocean biogeochemistry of the oligotrophic North Pacific Subtropical Gyre: from nutrient sources to carbon export. Rev. Geophys. 61, e2022RG000800. https://doi.org/10.1029/2022rg000800.

DeVries, T., Deutsch, C., 2014. Large-scale variations in the stoichiometry of marine organic matter respiration. Nat. Geosci. 7, 890–894. https://doi.org/10.1038/ngeo2300.

Feng, Y., Roleda, M.Y., Armstrong, E., Law, C.S., Boyd, P.W., Hurd, C.L., 2018. Environmental controls on the elemental composition of a Southern Hemisphere strain of the coccolithophore *Emiliania huxleyi*. Biogeosciences 15, 581–595. https://doi.org/10.5194/bg-15-581-2018.

Follett, C.L., White, A.E., Wilson, S.T., Follows, M.J., 2018. Nitrogen fixation rates diagnosed from diurnal changes in elemental stoichiometry. Limnol. Oceanogr. 63, 1911–1923. https://doi.org/10.1002/lno.10815.

Frigstad, H., Andersen, T., Hessen, D.O., Naustvoll, L.J., Johnsen, T.M., Bellerby, R.G.J., 2011. Seasonal variation in marine C:N:P stoichiometry: can the composition of seston explain stable Redfield ratios. Biogeosciences 8, 2917–2933. https://doi.org/10.5194/bg-8-2917-2011.

Fulweiler, R.W., 2023. More foxes than hedgehogs: the case for nitrogen fixation in coastal marine sediments. Glob. Biogeochem. Cycles 37, e2023GB007777. https://doi.org/10.1029/2023GB007777.

Garber, J.H., 1984. Laboratory study of nitrogen and phosphorus remineralization during the decomposition of coastal plankton and seston. Estuar. Coast. Shelf Sci. 18, 685–702. https://doi.org/10.1016/0272-7714(84)90039-8.

Garcia, C.A., Baer, S.E., Garcia, N.S., Rauschenberg, S., Twining, B.S., Lomas, M.W., Martiny, A.C., 2018. Nutrient supply controls particulate elemental concentrations and ratios in the low latitude eastern Indian Ocean. Nat. Commun. 9, 4868. https://doi.org/10.1038/s41467-018-06892-w.

Garcia, N.S., Bonachela, J.A., Martiny, A.C., 2016. Interactions between growth-dependent changes in cell size, nutrient supply and cellular elemental stoichiometry of marine *Synechococcus*. ISME J. 10, 2715–2724. https://doi.org/10.1038/ismej.2016.50.

Geider, R., Roche, J.L., 2002. Redfield revisited: variability of C:N:P in marine microalgae and its biochemical basis. Eur. J. Phycol. 37, 1–17. https://doi.org/10.1017/S0967026201003456.

GEOTRACES Intermediate Data Product Group, 2021. The GEOTRACES Intermediate Data Product 2021 (IDP2021). In: NERC EDS British Oceanographic Data Centre NOC. https://doi.org/10.5285/cf2d9ba9-d51d-3b7c-e053-8486abc0f5fd.

Gordon, D.C., 1971. Distribution of particulate organic carbon and nitrogen at an oceanic station in the Central Pacific, Deep Sea Res. Oceanogr. Abstr. 18, 1127–1134. https://doi.org/10.1016/0011-7471(71)90098-2.

Gradoville, M.R., Farnelid, H., White, A.E., Turk-Kubo, K.A., Stewart, B., Ribalet, F., Ferrón, S., Pinedo-Gonzalez, P., Armbrust, E.V., Karl, D.M., 2020. Latitudinal constraints on the abundance and activity of the cyanobacterium UCYN-A and other marine diazotrophs in the North Pacific. Limnol. Oceanogr. 65, 1858–1875. https://doi.org/10.1002/lno.11423.

Grasse, P., Closset, I., Jones, J., Geilert, S., Brzezinski, M., 2020. Controls on dissolved silicon isotopes along the US GEOTRACES Eastern Pacific Zonal Transect (GP16). Glob. Biogeochem. Cycles 34, e2020GB006538. https://doi.org/10.1029/2020GB006538.

Hashihama, F., Furuya, K., Kitajima, S., Takeda, S., Takemura, T., Kanda, J., 2009. Macro-scale exhaustion of surface phosphate by dinitrogen fixation in the western North Pacific. Geophys. Res. Lett. 36, L03610. https://doi.org/10.1029/2008GL036866.

Hebel, D.V., Karl, D.M., 2001. Seasonal, interannual and decadal variations in particulate matter concentrations and composition in the subtropical North Pacific Ocean. Deep Sea Res. Part II Top. Stud. Oceanogr. 48, 1669–1695. https://doi.org/10.1016/S0967-0645(00)00155-7.

Heldal, M., Scanlan, D.J., Norland, S., Thingstad, F., Mann, N.H., 2003. Elemental composition of single cells of various strains of marine *Prochlorococcus* and *Synechococcus* using X-ray microanalysis. Limnol. Oceanogr. 48, 1732–1743. https://doi.org/10.4319/lo.2003.48.5.1732.

Ho, T.Y., Quigg, A., Finkel, Z.V., Milligan, A.J., Wyman, K., Falkowski, P.G., Morel, F.M., 2003. The Elemental composition of some marine phytoplankton. J. Phycol. 39, 1145–1159. https://doi.org/10.1111/j.0022-3646.2003.03-090.x.

Iida, Y., Takatani, Y., Kojima, A., Ishii, M., 2021. Global trends of ocean CO_2 sink and ocean acidification: an observation-based reconstruction of surface ocean inorganic carbon variables. J. Oceanogr. 77, 323–358. https://doi.org/10.1007/s10872-020-00571-5.

Kemp, A.E., Villareal, T.A., 2013. High diatom production and export in stratified waters-a potential negative feedback to global warming. Prog. Oceanogr. 119, 4–23. https://doi.org/10.1016/j.pocean.2013.06.004.

Kessler, W.S., 2006. The circulation of the eastern tropical Pacific: a review. Prog. Oceanogr. 69, 181–217. https://doi.org/10.1016/j.pocean.2006.03.009.

Kitajima, S., Furuya, K., Hashihama, F., Takeda, S., Kanda, J., 2009. Latitudinal distribution of diazotrophs and their nitrogen fixation in the tropical and subtropical western North Pacific. Limnol. Oceangor. 54, 537–547. https://doi.org/10.4319/lo.2009.54.2.0537.

Knauer, G.A., Martin, J.H., Bruland, K.W., 1979. Fluxes of particulate carbon, nitrogen, and phosphorus in the upper water column of the Northeast Pacific. Deep Sea Res. Part A. Oceanogr. Res. Pap. 26, 97–108. https://doi.org/10.1016/0198-0149(79)90089-X.

Lam, P.J., Ohnemus, D.C., Auro, M.E., 2015. Size-fractionated major particle composition and concentrations from the US GEOTRACES North Atlantic zonal transect. Deep-Sea Res. II Top. Stud. Oceanogr. 116, 303–320. https://doi.org/10.1016/j.dsr2.2014.11.020.

Lam, P.J., Lee, J.M., Heller, M.I., Mehic, S., Xiang, Y., Bates, N.R., 2018. Size-fractionated distributions of suspended particle concentration and major phase composition from the US GEOTRACES Eastern Pacific Zonal Transect (GP16). Mar. Chem. 201, 90–107. https://doi.org/10.1016/j.marchem.2017.08.013.

Lee, J.M., Heller, M.I., Lam, P.J., 2018. Size distribution of particulate trace elements in the U.S. GEOTRACES Eastern Pacific Zonal Transect (GP16). Mar. Chem. 201, 108–123. https://doi.org/10.1016/j.marchem.2017.09.006.

Leonardos, N., Geider, R.J., 2004. Responses of elemental and biochemical composition of Chaetoceros muelleri to growth under varying light and nitrate: phosphate supply ratios and their influence on critical N:P. Limnol. Oceanogr. 49, 2105–2114. https://doi.org/10.4319/lo.2004.49.6.2105.

Letscher, R.T., Moore, J.K., 2015. Preferential remineralization of dissolved organic phosphorus and non-Redfield DOM dynamics in the global ocean: Impacts on marine productivity, nitrogen fixation, and carbon export. Glob. Biogeochem. Cycles 29, 325–340. https://doi.org/10.1002/2014GB004904.

Li, Q., Legendre, L., Jiao, N., 2015. Phytoplankton responses to nitrogen and iron limitation in the tropical and subtropical Pacific Ocean. J. Plankton Res. 37, 306–319. https://doi.org/10.1093/plankt/fbv008.

Liefer, J.D., White, A.E., Finkel, Z.V., Irwin, A.J., Dugenne, M., Inomura, K., Ribalet, F., Armbrust, E.V., Karl, D.M., Fyfe, M.H., Brown, C.M., Follows, M.J., 2024. Latitudinal patterns in ocean C:N:P reflect phytoplankton acclimation and macromolecular composition. Proc. Natl. Acad. Sci. USA 121, e2404460121. https://doi.org/10.1073/pnas.2404460121.

Liu, J., Song, J., Yuan, H., Li, X., Li, N., Duan, L., 2019. Biogenic matter characteristics, deposition flux correction, and internal phosphorus transformation in Jiaozhou Bay, North China. J. Mar. Syst. 196, 1–13. https://doi.org/10.1016/j.jmarsys.2019.04.001.

Liu, R., Wang, M., Li, W., Shi, X., Chen, T., 2020. Dissolved thorium isotope evidence for export productivity in the subtropical North Pacific during the late Quaternary. Geophys. Res. Lett. 47, GL085995. https://doi.org/10.1029/2019GL085995.

Lomas, M.W., Baer, S.E., Mouginot, C., Terpis, K.X., Lomas, D.A., Altabet, M.A., Martiny, A.C., 2021. Varying influence of phytoplankton biodiversity and stoichiometric plasticity on bulk particulate stoichiometry across ocean basins. Commun. Earth Environ. 2, 143. https://doi.org/10.1038/s43247-021-00212-9.

Martiny, A., Vrugt, J.A., Primeau, F.W., Lomas, M.W., 2013a. Regional variation in the particulate organic carbon to nitrogen ratio in the surface ocean. Glob. Biogeochem. Cycles 27, 723–731. https://doi.org/10.1002/gbc.20061.

Martiny, A.C., Pham, C.T., Primeau, F.W., Vrugt, J.A., Moore, J.K., Levin, S.A., Lomas, M. W., 2013b. Strong latitudinal patterns in the elemental ratios of marine plankton and organic matter. Nat. Geosci. 6, 279–283. https://doi.org/10.1038/NGEO1757.

Martiny, A.C., Ma, L., Mouginot, C., Chandler, J.W., Zinser, E.R., 2016. Interactions between thermal acclimation, growth rate, and phylogeny influence *Prochlorococcus* elemental stoichiometry. PLoS One 11, e0168291. https://doi.org/10.1371/journal.pone.0168291.

Matsumoto, K., Tanioka, T., 2020. Shifts in regional production as a driver of future global ocean production stoichiometry. Environ. Res. Lett. 15, 124027. https://doi.org/10.1088/1748-9326/abc4b0.

Matsumoto, K., Rickaby, R., Tanioka, T., 2020a. Carbon export buffering and CO_2 drawdown by flexible phytoplankton C:N:P under glacial conditions. Paleoceanogr. Paleoclimatol. 35, e2019PA003823. https://doi.org/10.1029/2019PA003823.

Matsumoto, K., Tanioka, T., Rickaby, R., 2020b. Linkages between dynamic phytoplankton C:N:P and the ocean carbon cycle under climate change. Oceanography 33, 44–52. https://doi.org/10.5670/oceanog.2020.203.

Matsumoto, K., Sasai, Y., Sasaoka, K., Siswanto, E., Honda, M.C., 2021. The formation of subtropical phytoplankton blooms is dictated by water column stability during winter and spring in the oligotrophic northwestern North Pacific. J. Geophys. Res. Oceans 126, e2020JC016864. https://doi.org/10.1029/2020JC016864.

Minor, E.C., Eglinton, T.I., Olson, R., Boon, J.J., 1998. The compositional heterogeneity of particulate organic matter from the surface ocean: an investigation using flow cytometry and DT-MS. Org. Geochem. 29, 1561–1582. https://doi.org/10.1016/S0146-6380(98)00161-2.

Moreno, A.R., Martiny, A.C., 2018. Ecological stoichiometry of ocean plankton. Annu. Rev. Mar. Sci. 10, 43–69. https://doi.org/10.1146/annurev-marine-121916-063126.

Mouginot, C., Zimmerman, A.E., Bonachela, J.A., Fredricks, H., Allison, S.D., Van Mooy, B.A., Martiny, A.C., 2015. Resource allocation by the marine cyanobacterium *Synechococcus* WH8102 in response to different nutrient supply ratios. Limnol. Oceanogr. 60, 1634–1641. https://doi.org/10.1002/lno.10123.

Ohnemus, D.C., Auro, M.E., Sherrell, R.M., Lagerstrom, M., Morton, P.L., Twining, B.S., Rauschenberg, S., Lam, P.J., 2014. Laboratory intercomparison of marine particulate digestions including Piranha: a novel chemical method for dissolution of polyether sulfone filters. Limnol. Oceanogr. Methods 12, 530–547. https://doi.org/10.4319/lom.2014.12.530.

Ohnemus, D.C., Rauschenberg, S., Cutter, G.A., Fitzsimmons, J.N., Sherrell, R.M., Twining, B.S., 2017. Elevated trace metal content of prokaryotic communities associated with marine oxygen deficient zones. Limnol. Oceanogr. 62, 3–25. https://doi.org/10.1002/lno.10363.

Peters, B.D., Lam, P.J., Casciotti, K.L., 2018. Nitrogen and oxygen isotope measurements of nitrate along the US GEOTRACES Eastern Pacific Zonal Transect (GP16) yield insights into nitrate supply, remineralization, and water mass transport. Mar. Chem. 201, 137–150. https://doi.org/10.1016/j.marchem.2017.09.009.

Piper, M.M., Benitez-Nelson, C.R., Frey, K.E., Mills, M.M., Pal, S., 2016. Dissolved and particulate phosphorus distributions and elemental stoichiometry throughout the Chukchi Sea. Deep-Sea Res. II Top. Stud. Oceanogr. 130, 76–87. https://doi.org/10.1016/j.dsr2.2016.05.009.

Polovina, J.J., Howell, E.A., Abecassis, M., 2008. Ocean's least productive waters are expanding. Geophys. Res. Lett. 35, L03618. https://doi.org/10.1029/2007GL031745.

Pujo-Pay, M., Conan, P., Oriol, L., Cornet-Barthaux, V., Falco, C., Ghiglione, J.F., Goyet, C., Moutin, T., Prieur, L., 2011. Integrated survey of elemental stoichiometry (C, N, P) from the western to eastern Mediterranean Sea. Biogeosciences 8, 883–899. https://doi.org/10.5194/bg-8-883-2011.

Quay, P., 2021. Impact of the elemental composition of exported organic matter on the observed dissolved nutrient and trace element distributions in the upper layer of the ocean. Glob. Biogeochem. Cycles 35, e2020GB006902. https://doi.org/10.1029/2020GB006902.

Quigg, A., Finkel, Z.V., Irwin, A.J., Rosenthal, Y., Ho, T.Y., Reinfelder, J.R., Schofield, O., Morel, F.M.M., Falkowski, P.G., 2003. The evolutionary inheritance of elemental stoichiometry in marine phytoplankton. Nature 425, 291–294. https://doi.org/10.1098/rspb.2010.1356.

Ragueneau, O., Schultes, S., Bidle, K., Claquin, P., Moriceau, B., 2006. Si and C interactions in the world ocean: Importance of ecological processes and implications for the role of diatoms in the biological pump. Glob. Biogeochem. Cycles 20, GB4S02. https://doi.org/10.1029/2006GB002688.

Redfield, A.C., 1934. On the proportions of organic derivatives in seawater and the irrelation to the composition of plankton. In: James Johnstone Memorial Volume. University of Liverpool Press, Liverpool, pp. 176–192.

Rhee, G.Y., 1978. Effects of N:P atomic ratios and nitrate limitation on algal growth, cell composition, and nitrate uptake. Limnol. Oceanogr. 23, 10–25. https://doi.org/10.4319/lo.1978.23.1.0010.

Schneider, B., Schlitzer, R., Fischer, G., Nöthig, E.M., 2003. Depth-dependent elemental compositions of particulate organic matter (POM) in the ocean. Glob. Biogeochem. Cycles 17, 1032. https://doi.org/10.1029/2002GB001871.

Shaffer, G., Bendtsen, J., Ulloa, O., 1999. Fractionation during remineralization of organic matter in the ocean. Deep Sea Res. I: Oceanogr. Res. Pap. 46, 185–204. https://doi.org/10.1016/S0967-0637(98)00061-2.

Shao, Z., Xu, Y., Wang, H., Luo, W., Wang, L., Huang, Y., Agawin, N.S.R., Ahmed, A., Benavides, M., Bentzon-Tilia, M., Berman Frank, I., Berthelot, H., Biegala, I.C., Bif, M.B., Bode, A., Bonnet, S., Bronk, D.A., Brown, M.V., Campbell, L., Capone, D.G., Carpenter, E.J., Cassar, N., Chang, B.X., Chappell, D., Chen, Y.L., Church, M.J., Cornejo-Castillo, F.M., Detoni, A.M.S., Doney, S.C., Dupouy, C., Estrada, M., Fernandez, C., Fernández-Castro, B., Fonseca-Batista, D., Foster, R.A., Furuya, K., Garcia, N., Goto, K., Gago, J., Gradoville, M.R., Hamersley, M.R., Henke, B.A., Hörstmann, C., Jayakumar, A., Jiang, Z., Kao, S.J., Karl, D.M., Kittu, L.R., Knapp, A. N., Kumar, S., LaRoche, J., Liu, H., Liu, J., Lory, C., Löscher, C.R., Marañón, E., Messer, L.F., Mills, M.M., Mohr, W., Moisander, P.H., Ma haffey, C., Moore, R., Mouriño-Carballido, B., Mulholland, M.R., Nakaoka, S., Needoba, J.A., Raes, E.J., Rahav, E., Ramírez Cárdenas, T., Reeder, C.F., Riemann, L., Riou, V., Robidart, J.C., Sarma, V.V.S.S., Sato, T., Saxena, H., Selden, C., Seymour, J.R., Shi, D., Shiozaki, T., Singh, A., Sipler, R.E., Sun, J., Suzuki, K., Takahashi, K., Tan, Y., Tang, W., Tremblay, J.É., Turk-Kubo, K., Wen, Z., White, A.E., Wilson, S.T., Yoshida, T., Zehr, J.P., Zhang, R., Zhang, Y., Luo, Y.W., 2023. Global oceanic diazotroph database version 2 and elevated estimate of global oceanic N_2 fixation. Earth Syst. Sci. Data 15, 3673–3709. https://doi.org/10.5194/essd-15-3673-2023.

Sharoni, S., Halevy, I., 2020. Nutirent ratios in marine particulate organic matter are predicted by the population structure of well-adapted phytoplankton. Sci. Adv. 6, eaaw9371. https://doi.org/10.1126/sciadv.aaw9371.

Shelley, R.U., Morton, P.L., Landing, W.M., 2015. Elemental ratios and enrichment factors in aerosols from the us-geotraces North Atlantic transects. Deep-Sea Res. II Top. Stud. Oceanogr. 116, 262–272. https://doi.org/10.1016/j.dsr2.2014.12.005.

Shiozaki, T., Furuya, K., Kodama, T., Kitajima, S., Takeda, S., Takemura, T., Kanda, J., 2010. New estimation of N_2 fixation in the western and Central Pacific Ocean and its marginal seas. Glob. Biogeochem. Cycles 24, GB1015. https://doi.org/10.1029/2009GB003620.

Slomp, C.P., Thomson, J., de Lange, G.J., 2004. Controls on phosphorus regeneration and burial during formation of eastern Mediterranean sapropels. Mar. Geol. 203, 141–159. https://doi.org/10.1016/S0025-3227(03)00335-9.

Sterner, R.W., Andersen, T., Elser, J.J., Hessen, D.O., Hood, J.M., McCauley, E., Urabe, J., 2008. Scale-dependent carbon:nitrogen:phosphorus seston stoichiometry in marine and freshwaters. Limnol. Oceanogr. 53, 1169–1180. https://doi.org/10.4319/lo.2008.53.3.1169.

Subhas, A.V., Pavia, F.J., Dong, S., Lam, P.J., 2023. Global trends in the distribution of biogenic minerals in the ocean. J. Geophys. Res. Oceans 128, e2022JC019470. https://doi.org/10.1029/2022JC019470.

Takahashi, T., Sutherland, S.C., Wanninkhof, R., Sweeney, C., Feely, R.A., Chipman, D. W., Hales, B., Friederich, G., Chavez, F., Sabine, C., Watson, A., Bakker, D.C., Schuster, U., Metzl, N., Yoshikawa-Inoue, H., Ishii, M., Midorikawa, T., Nojiri, Y., Körtzinger, A., Steinhoff, T., Hoppema, M., Olafsson, J., Arnarson, T.S., Tilbrook, B., Johannessen, T., Olsen, A., Bellerby, R., Wong, C., Delille, B., Bates, N., de Baar, H.J., 2009. Climatological mean and decadal changes in surface ocean pCO_2, and net sea-air CO_2 flux over the global oceans. Deep Sea Res. Part II Top. Stud. Oceanogr. 56, 554–577. https://doi.org/10.1016/j.dsr2.2008.12.009.

Talmy, D., Martiny, A., Hill, C., Hickman, A., Follows, M., 2016. Microzooplankton regulation of surface ocean POC:PON ratios. Glob. Biogeochem. Cycles 30, 311–332. https://doi.org/10.1002/2015GB005273.

Tang, W., Li, Z., Cassar, N., 2019. Machine learning estimates of global marine nitrogen fixation. J. Geophys. Res. Biogeosci. 124, 717–730. https://doi.org/10.1029/2018JG004828.

Tanioka, T., Matsumoto, K., 2020. A meta-analysis on environmental drivers of marine phytoplankton C:N:P. Biogeosciences 17, 2939–2954. https://doi.org/10.5194/bg-17-2939-2020.

Tanioka, T., Garcia, C.A., Larkin, A.A., Garcia, N.S., Fagan, A.J., Martiny, A.C., 2022. Global patterns and predictors of C:N:P in marine ecosystems. Commun. Earth Environ. 3, 271. https://doi.org/10.1038/s43247-022-00603-6.

Teng, Y.C., Primeau, F.W., Moore, J.K., Lomas, M.W., Martiny, A.C., 2014. Global-scale variations of the ratios of carbon to phosphorus in exported marine organic matter. Nat. Geosci. 7, 895–898. https://doi.org/10.1038/NGEO2303.

Tréguer, P., Bowler, C., Moriceau, B., Dutkiewicz, S., Gehlen, M., Aumont, O., Bittner, L., Dugdale, R., Finkel, Z., Iudicone, D., 2018. Influence of diatom diversity on the ocean biological carbon pump. Nat. Geosci. 11, 27–37. https://doi.org/10.1038/s41561-017-0028-x.

Twining, B.S., Rauschenberg, S., Morton, P.L., Vogt, S., 2015. Metal contents of phytoplankton and labile particulate material in the North Atlantic Ocean. Prog. Oceanogr. 137, 261–283. https://doi.org/10.1016/j.pocean.2015.07.001.

Van Mooy, B.A., Devol, A.H., 2008. Assessing nutrient limitation of *Prochlorococcus* in the North Pacific subtropical gyre by using an RNA capture method. Limnol. Oceanogr. 53, 78–88. https://doi.org/10.4319/lo.2008.53.1.0078.

Wang, W.L., Moore, J.K., Martiny, A.C., Primeau, F.W., 2019. Convergent estimates of marine nitrogen fixation. Nature 566, 205–211. https://doi.org/10.1038/s41586-019-0911-2.

Wen, Z., Browning, T.J., Cai, Y., Dai, R., Zhang, R., Du, C., Jiang, R., Lin, W., Liu, X., Cao, Z., 2022. Nutrient regulation of biological nitrogen fixation across the tropical western North Pacific. Sci. Adv. 8, eabl7564. https://doi.org/10.1126/sciadv.abl7564.

Winn, C.D., Mackenzie, F.T., Carrillo, C.J., Sabine, C.L., Karl, D.M., 1994. Air-sea carbon dioxide exchange in the North Pacific Subtropical Gyre: Implications for the global carbon budget. Glob. Biogeochem. Cycles 8, 157–163. https://doi.org/10.1029/94GB00387.

Xu, Z., Wang, B., Luo, Y., Li, H., Zhang, J., Jin, H., Chen, J., 2021. Changes of carbon to nitrogen ratio in particulate organic matter in the marine mesopelagic zone: a case from the South China Sea. Mar. Chem. 231, 103930. https://doi.org/10.1016/j.marchem.2021.103930.

Yang, J.Y.T., Kao, S.J., Dai, M., Yan, X., Lin, H.L., 2017. Examining N cycling in the northern South China Sea from N isotopic signals in nitrate and particulate phases. J. Geophys. Res. Biogeosci. 122, 2118–2136. https://doi.org/10.1002/2016JG003618.

Yuan, Z., Browning, T.J., Zhang, R., Wang, C., Du, C., Wang, Y., Chen, Y., Liu, Z., Liu, X., Shi, D., Dai, M., 2023. Potential drivers and consequences of regional phosphate depletion in the western subtropical North Pacific. Limnol. Oceanogr. Lett. 8, 509–518. https://doi.org/10.1002/lol2.10314.

Zhang, C., Wang, Y., Bi, R., Sommer, U., Song, G., Chen, Z., Lin, F., Zhang, J., Zhao, M., 2024a. C:N stoichiometry and the fate of organic carbon in ecosystems of the northwest Pacific Ocean. Prog. Oceanogr. 229, 103372. https://doi.org/10.1016/j.pocean.2024.103372.

Zhang, J., Li, M., Xu, L., Zhu, J., Dai, G., He, N., 2021. C:N:P stoichiometry in terrestrial ecosystems in China. Sci. Total Environ. 795, 148849. https://doi.org/10.1016/j.scitotenv.2021.148849.

Zhang, K., Zhou, K., Cai, Y., Yuan, Z., Chen, Y., Xu, F., Liu, X., Cao, Z., Dai, M., 2024b. Decoupled cycling of particulate cadmium and phosphorus in the subtropical Northwest Pacific. Limnol. Oceanogr. 69, 1941–1954. https://doi.org/10.1002/lno.12635.

Zhou, K., Dai, M., Kao, S.J., Wang, L., Xiu, P., Chai, F., Tian, J., Liu, Y., 2013. Apparent enhancement of ^{234}Th-based particle export associated with anticyclonic eddies. Earth Planet. Sci. Lett. 381, 198–209. https://doi.org/10.1016/j.epsl.2013.07.039.